# Early Carboniferous Unroofing in Western Norway: A Tale of Alkali Feldspar Thermochronology

*E. A. Eide, T. H. Torsvik,*[1] *T. B. Andersen,*[2] *and N. O. Arnaud*[3]

*Geological Survey of Norway, N-7491 Trondheim, Norway*
(*e-mail: Elizabeth.Eide@ngu.no*)

**ABSTRACT**

$^{40}Ar/^{39}Ar$ thermochronologic data from an extensional detachment zone in western Norway document punctuated late Paleozoic through Mesozoic tectonothermal activity. Diffusion and thermal modeling of alkali feldspars sampled in a profile through the detachment replicate laboratory argon release patterns when feldspars comprise three or four diffusion domains with differing activation energies that represent high-, intermediate-, and low-closure temperatures. These domains correspond to distinct changes in late Paleozoic cooling rates: (1) slow cooling at 0.4°–2.2°C/m.yr. from ca. 380–360 Ma; (2) rapid cooling at ≥15°C/m.yr. in Late Devonian–Early Carboniferous time (360–340 Ma); (3) slow cooling at 0.4°–1.7°C/m.yr. after ca. 340 Ma, with partial argon loss in Permian and Late Jurassic–Early Cretaceous times. The Early Carboniferous rapid cooling event recorded by the feldspars links the western Norway margin to contemporaneous unconformities, regional extension, basin inversion, and igneous activity previously identified around the proto–North Atlantic perimeter. We attribute this Early Carboniferous rapid cooling event in western Norway to an episode of unroofing. Unroofing was a consequence of increased topography and erosion; movement of the rocks toward the surface (higher topography) may have been triggered by thermal underplating combined with regional, transcurrent tectonics. The results support the judicious application of multidiffusion domain analysis of Ar-Ar alkali feldspar data from areas with well-constrained tectonostratigraphy and other, independent means of age control.

## Introduction

The post-Caledonian evolution of the northern North Atlantic region is derived by linking the post-Caledonian onshore histories of eastern Laurentia, Avalonia, Baltica, and Barentsia with offshore seismic and well data. The post-Caledonian evolution of western Baltica has been a somewhat peripheral actor in developing these tectonic models because of its paucity of onshore, post-Devonian rocks. Available chronologic markers for post-Caledonian, onshore western Baltica presently are composed of a few absolute ages from young, brittle faults and Late Permian dikes, the occurrence of Jurassic sediments in isolated pockets, and tectonothermal information available from the Permo-Carboniferous Oslo Rift region (fig. 1; Færseth et al. 1976; Løvlie and Mitchell 1982; Bøe and Bjerkli 1989; Torsvik et al. 1992, 1997; Rohrman et al. 1994; Sundvoll and Larsen 1994; Eide et al. 1997; Fossen et al. 1997; Dunlap and Fossen 1998). These geographically and chronologically discontinuous pieces of information contrast with well-exposed late Paleozoic and Mesozoic sediments, volcanic rocks, and fault-basins on East Greenland, Svalbard, and the British Isles (Haszeldine 1984; Steel and Worsley 1984; Ziegler 1990; Coward 1993; Bergh et al. 1997; Hartz et al. 1997). The thermotectonic history of Baltica is an obvious but relatively unconstrained player in models of the post-Caledonian North Atlantic region.

The thermal history of the exposed Baltican crust can be used as a proxy for (missing) post-Devonian rocks onshore and may be tracked via judicious application of thermochronology. $^{40}Ar/^{39}Ar$ alkali feldspar thermochronology and multidiffusion do-

Manuscript received June 25, 1998; accepted February 18, 1999.

[1] Institute for Solid Earth Geophysics, University of Bergen, Allegate 41, 5007 Bergen, Norway.

[2] Department of Geology, University of Oslo, P.O. Box 1047, 0316 Blindern, Oslo 3, Norway.

[3] Université Blaise Pascal, UMR 5624 du CNRS, Laboratoire de Geologie, 5 rue Kessler, 63038 Clermont-Ferrand CEDEX, France.

[The Journal of Geology, 1999, volume 107, p. 353–374]  0022-1376/99/10703-0007$01.00

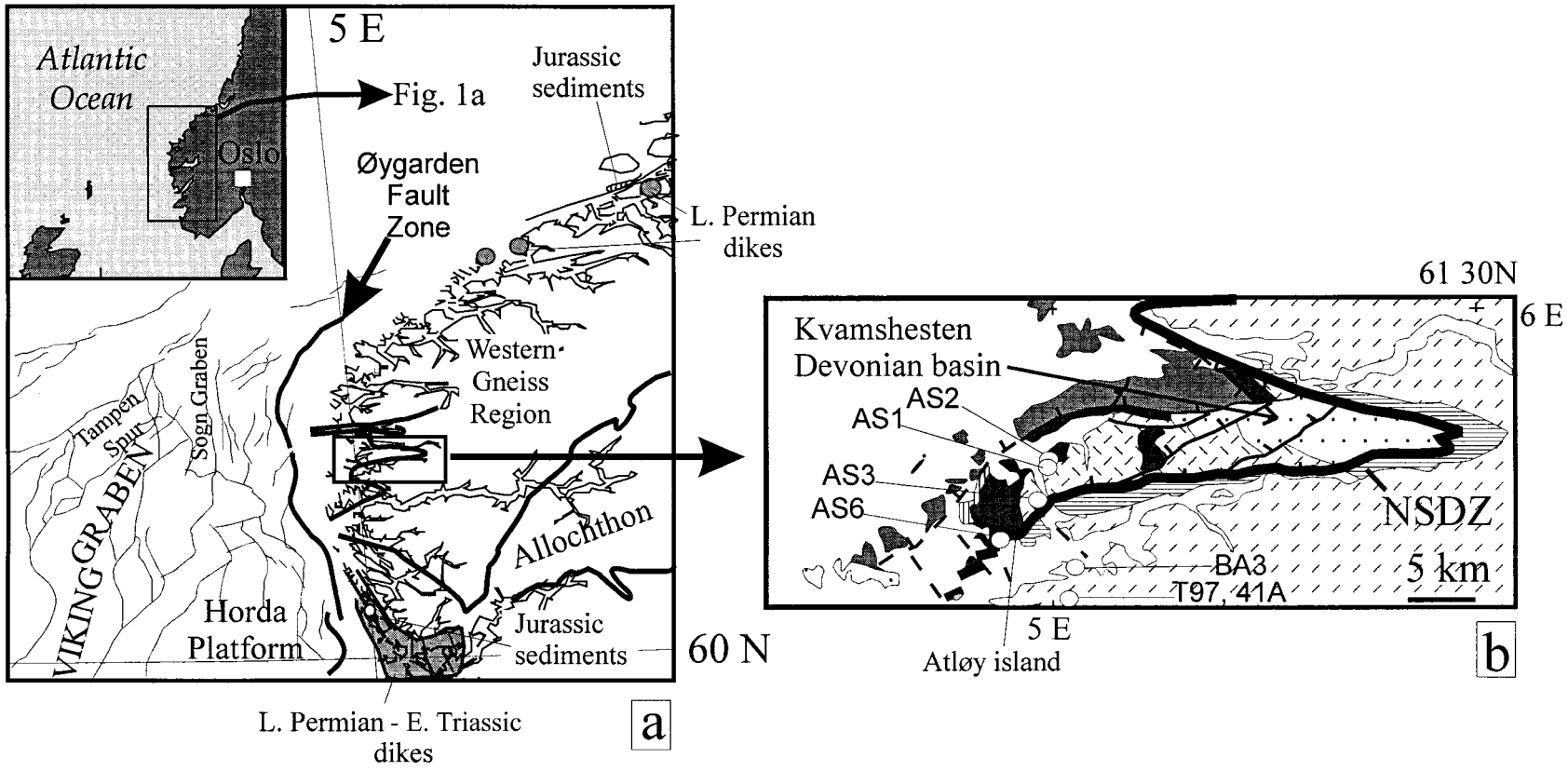


**Figure 1.** Regional and local geology map for western Norway study area. *a*, Study area relative to the Western Gneiss Region (WGR) and offshore basement lineaments. Major faults are shown in thick black lines. Gray shaded zones onshore denote areas with late Paleozoic and Mesozoic dikes. Near-shore Jurassic sediment locations are noted. *b*, Sample localities (*white dots*) cross a tectonostratigraphic profile through the Nordfjord-Sogn Detachment Zone (NSDZ). The key to the patterns is in figure 2. Patterns and shaded units to the west of NSDZ are allochthonous, while the diagonal dash pattern to the east denotes basement.

main (MDD) analysis have been used successfully elsewhere to document cooling and unroofing histories and ages of fault motions (e.g., Lovera et al. 1989; Copeland et al. 1991; Arnaud et al. 1993). Nonetheless, use of cooling histories modeled from feldspar argon data remains a contentious method in tectonic studies because of ongoing debate about mechanisms of argon diffusion in feldspars and the inherent assumptions necessary to extrapolate the laboratory modeling results to natural feldspar behavior (Lovera et al. 1989, 1991; Foland and Xu 1990; Burgess et al. 1992; Villa 1994; Arnaud and Kelley 1997).

Notwithstanding, and in part because of, these arguments, we have applied MDD analysis to argon data from isothermal, cycled heating experiments on alkali feldspars from western Norway following the method of Lovera et al. (1989, 1991). The rocks derive from a tightly constrained tectonostratigraphic profile through a major extensional detachment, and the resulting data are significant for two reasons: (1) they document a heretofore unknown rapid cooling event in Late Devonian–Early Carboniferous time (340–360 Ma) in western Norway (time scales of Gradstein and Ogg [1996] and Tucker et al. [1998]); and (2) they are most easily and reasonably explained to represent argon release from several (three to four) diffusion domains of varying sizes and activation energies. The age data and cooling histories are consistent with events of similar age previously documented in the Barents Sea region, East Greenland, and Britain and promote multidomain, volume diffusion as a viable process governing argon transport and storage in at least some natural alkali feldspars.

## Geologic Setting

The samples were taken from a profile through the Nordfjord-Sogn Detachment Zone (NSDZ) in the Sunnfjord region of western Norway (figs. 1, 2). The Caledonian history of the area involved a subduction-collision sequence between a rapidly moving Baltican continent and nearly stationary Laurentia from latest Ordovician to earliest Devonian (ca. 450–410 Ma) times; this process generated high- to ultra-high-pressure (HP-UHP) rocks in the subducted Baltican crust (western Norway) and HP rocks in the allochthonous nappes now exposed on the Baltican margin (Smith 1984; Dobrzhinetskaya et al. 1995; Boundy et al. 1996; Torsvik et al. 1996; Wain 1997; Andersen 1998; Andersen et al. 1998; Fossen and Dunlap 1998). Exhumation of the HP-UHP Baltican crust occurred primarily during and shortly after collision and was later abetted at higher crustal levels by extensional collapse along a series of detachments, possibly aided by slab delamination (Andersen and Jamtveit 1990; Andersen et al. 1991, 1994; Dewey et al. 1993).

Exhumation of HP-UHP rocks in Early through Middle Devonian times in western Norway was coeval with deposition of fluvial-alluvial clastic sediments in basins sourced in the allochthonous nappes (Hossack 1984; Osmundsen and Andersen 1994; Osmundsen et al. 1998). The postcollisional crustal thinning and top-west transport of the nappe piles juxtaposed the HP, eclogite-bearing basement of the Western Gneiss Region with middle and upper crustal allochthonous constituents and Devonian Basins and is now manifested by the 2–3-km-thick extensional mylonite of the NSDZ (figs. 1, 2; Andersen and Jamtveit 1990; Fossen 1992).

As background to this study, we point to some anomalous tectonostratigraphic relationships in this subduction-collision-exhumation-extension scenario that have remained unclarified in the literature and indicate significant, but enigmatic, post-Caledonian activity in western Norway. First, the Devonian Basins are now in contact with both high- and low-pressure units, despite the fact that the clasts of the basin sediments were sourced exclusively from a high crustal–level (allochthonous nappe) source (see fig. 1). Second, the entire tectonostratigraphy, including the Devonian Basins, is folded along east-west trending axes into a broad, anti-, and synformal series (fig. 1). Third, lower sections of the folded Devonian sediments are apparently metamorphosed to lower greenschist facies. Fourth, several generations of brittle faults cutting the area have been classified as either syndepositional (in the Devonian Basins), Late Permian and related to similarly aged mafic dikes occurring along near-shore western Norway (fig. 1), or Mesozoic and younger and related to the general east-west extensional regime active during offshore basin development and opening of the North Atlantic (Roberts 1983; Torsvik et al. 1986, 1992, 1997; Cuthbert 1991; Chauvet and Séranne 1994; Osmundsen and Andersen 1994; Eide et al. 1997; Fossen et al. 1997; Hartz and Andresen 1997; Osmundsen et al. 1998). The chronology of these events and their implications for post-Caledonian Baltica have been partially resolved by the current feldspar studies in western Norway.

## Sample Description

The focus on late Paleozoic and younger events in western Norway necessitated the use of thermo-

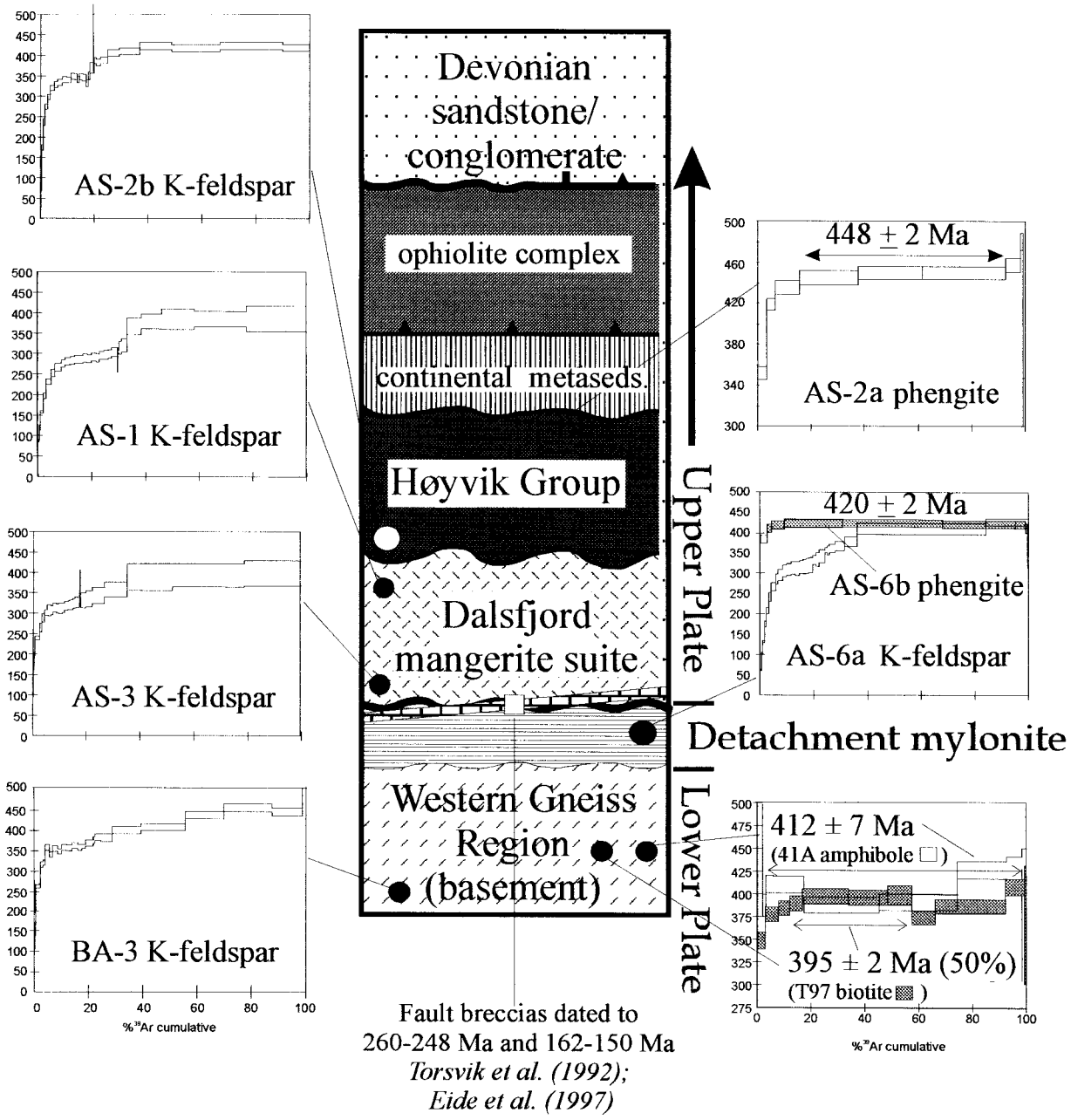


**Figure 2.** Tectonostratigraphic section and age spectra through the NSDZ, with rock patterns the same as figure 1*b*. Unit thicknesses not to scale. Tectonostratigraphy is modified after Osmundsen and Andersen (1994). Age spectra contain corresponding mineral and sample numbers. Note that we analyzed both mica and feldspar from two samples (*AS-2* and *AS-6*). See "$^{40}Ar/^{39}Ar$ Geochronology" text for details. Large uncertainties in the upper temperature steps of several experiments, especially in the high-temperature portions of the release spectra, were caused by unusually high high-temperature blanks on the day(s) of analysis; this was a function of the necessity to conduct the analyses soon after sample loading, before the blanks had resumed their normal operating levels of $5 \times 10^{-18}$ mol/min of $^{40}Ar$ (<1000°C). Sample sizes and signals at all steps were always sufficient to precisely measure the argon isotopes. Note change in age scale on a few of the spectra.

chronologic methods with low closure temperatures since the region was not heated above ca. 400°C since mid-Devonian time; much of the upper crustal allochthon, in fact, remained below 400°C since the Late Ordovician (Andersen et al. 1998). We utilized the advantage of low Ar-closure temperatures for slowly cooled alkali feldspars (ca. 400°–150°C; Lovera et al. 1991) to track the cooling histories of the rocks in a profile through the NSDZ. We have established that the structurally highest and lowest samples in the profile were isolated from the influence of advective heating or fluids associated with Permian and Mesozoic reactivation of the NSDZ (fig. 2; Eide et al. 1997). In addition to alkali feldspars, we also analyzed white micas, biotite, and amphibole from the same or associated rocks to establish boundary constraints (temperatures and times) for the alkali feldspar thermal and diffusion modeling.

The samples included rocks from the hanging wall of the NSDZ, from the detachment mylonite, and from the footwall, eclogite-bearing gneisses; they constitute, from structurally uppermost to lowermost (fig. 2), alkali feldspar and white mica from the Høyvik Group (AS-2a, AS-2b); two alkali feldspars from the Dalsfjord Mangerite Suite (AS-1 and AS-3); alkali feldspar and white mica from the detachment mylonites (AS-6a, AS-6b); and alkali feldspar (BA-3), biotite (T97), and barroisitic amphibole (41A) from several lithologies in the eclogite-bearing basement (figs. 1, 2). Brittle fault rocks from the fault on Atløy, cross-cutting the detachment, have also been dated with the Ar-Ar method (Eide et al. 1997). The structural and temporal relationships between the various tectonostratigraphic units are described in Brekke and Solberg (1987), Osmundsen and Andersen (1994), and Andersen et al. (1998).

***Høyvik Group.*** The Høyvik Group is a metapsammitic unit that unconformably overlies the Dalsfjord Suite and is unconformably overlain by the Silurian (Wenlock) Herland Group marine sedimentary package (fig. 2; Brekke and Solberg 1987; Osmundsen and Andersen 1994). Quartz is characterized by undulatory extinction and sutured grain boundaries, while alkali feldspar porphyroclasts have weakly undulatory extinction and smoothly curved grain boundaries; tabular phengites range from gently kinked to undeformed. Textural features suggest one episode of white mica growth and deformation at temperatures from 400°–450°C slightly before 448 Ma ($^{40}Ar/^{39}Ar$ cooling ages for phengite in the rocks; Andersen et al. 1998).

Sample AS-2 derives from the lowermost section of the Høyvik Group, ca. 50 m above the unconformable contact with the Dalsfjord Suite (figs. 1, 2). The rock constitutes an alkali feldspar-quartz-phengite-oxide gneiss with accessory titanite and pyrite and late, minor chlorite. The foliation is defined by thin layers of fairly coarse-grained phengite separating quartzofeldspathic bands. Feldspar porphyroclasts in the sample are microperthitic, coarse-grained, and asymmetrically flattened. Subgrain development is evident on grain rims, and fine oxide inclusions occur in grain cores.

***Dalsfjord Suite.*** The bulk of the Dalsfjord Suite is a crystalline unit of (presumed) Precambrian age and is composed of mangeritic syenite gneiss with minor granitic gneiss, anorthosite, and younger nongneissose gabbros (Kolderup 1921; Brekke and Solberg 1987). A late, greenschist facies overprint pervades the sequence, and the lowermost 50 m of the unit is brecciated in proximity to a brittle fault on Atløy (fig. 2; Brekke and Solberg 1987; Eide et al. 1997). One sample (AS-1) was taken ca. 20 m below the unconformable contact with the Høyvik Group (fig. 2). A second Dalsfjord Suite sample (AS-3) was taken from ca. 50 m above the fault on Atløy.

Sample AS-1 contains microcline, plagioclase, quartz, and oxides with accessory garnet and, in thin veins or pockets, a secondary, greenschist facies assemblage of titanite, white mica, chlorite, and biotite. While much of the rock preserves even grain boundaries and original igneous textures, some of the quartzofeldspathic minerals indicate partially recovered strain via subgrain zone development around alkali feldspar rims, strained twins in plagioclase, and polygonal quartz rinds around the coarsest alkali feldspar porphyroblasts. Notably, the rock lacks any evidence for brittle deformation, in contrast to AS-3 from the same unit but from a position lower in the tectonostratigraphy (see "The Nordfjord-Sogn Detachment and Mylonites"). Plagioclase feldspars are antiperthitic and clouded with fine-grained white mica, titanite, and/or epidote grains, related to the greenschist facies recrystallization.

Sample AS-3 has a mineral assemblage similar to AS-1 but is much more deformed (both ductiley and brittley). Grain boundaries are generally serrated and irregular, and the quartzofeldspathic minerals exhibit extensive subgrain growth. Microperthite is slightly turbid, and plagioclase porphyroblasts are clouded by fine-grained inclusions of white mica. Late Permian and Late Jurassic–Early Cretaceous brittle activity along the Atløy fault was accompanied by brittle fracturing of this rock and its associated very low–greenschist facies mineralization in thin veinlets (Torsvik et al. 1992; Eide

et al. 1997). Incipient autobrecciation is evident on some of the throughgoing microfractures in this rock.

***The Nordfjord-Sogn Detachment and Mylonites.*** The low- to medium-grade, highly strained rocks occur in the footwall of the detachment. The mylonitic to ultramylonitic foliation is punctuated by smeared, alkali feldspar augen. Kinematic indicators and microtextures in the mylonite here and elsewhere around the NSDZ document top-west or top-northwest shear sense (Andersen and Jamtveit 1990). Sample AS-6 was taken from ca. 50 m below the tectonic contact with the Upper Plate units (fig. 1) and is composed of alkali feldspar, quartz, and white mica, with minor oxides in a mylonite matrix. White micas are fairly coarse and have well-developed tabular habits with asymmetry in keeping with top-west sense of shear.

***Western Gneiss Region Units.*** Regionally, these rocks are a blend of granitic, granodioritic, and tonalitic gneisses, eclogites, and partially metamorphosed mafic igneous rocks (anorthosites, gabbros, and garnet-pyroxenites). Cuthbert and Carswell (1990) describe the eclogite-bearing gneisses in Sunnfjord. Sample BA-3 from the small island of Bårdsholmen is part of a Precambrian granulite facies complex (1000 ± 10 Ma; Gromet and Andersen 1994) metamorphosed to eclogite facies during Caledonian collision and subsequently retrogressed to amphibolite facies during exhumation (A. Engvik, personal communication).

Leucocratic granulite (BA-3) is composed of quartz, orthoclase, fine-grained white mica, and accessory oxides, epidote, and Cl-rich amphibole; biotite forms after white mica. Garnet and hypersthene also occur in some examples. The rock has a strong planar fabric where both quartz and feldspar are flattened along the foliation plane. Variably sized quartz grains have serrated boundaries and undulatory extinction, while coarser feldspar porphyroblasts have irregular extinction zones (partially healed subgrain regions). Feldspars have rare, very fine-grained mica inclusions.

Biotite T97 was separated from a pegmatite filling a top-west shear zone in tonalitic basement gneisses. The pegmatite is composed of the assemblage biotite, albite, and quartz. Barroisitic amphibole sample 41A was separated from a monomineralic vein cutting an eclogite body in Sunnfjord.

## $^{40}Ar/^{39}Ar$ Geochronology

***Analytical Procedures.*** High-purity mineral separates for $^{40}Ar/^{39}Ar$ analysis were prepared by standard crushing, separating, and cleaning techniques. Analytical protocol was similar to Arnaud et al. (1993; also table 1), with analyses performed on a VG3600 mass spectrometer. Individual steps are listed in tables at the $1\sigma$ confidence level without error in $J$ value (1%–2%); plateau and isochron ages are reported at $2\sigma$ without uncertainty in $J$ value. A plateau is defined when the ages from three or more contiguous steps comprise >50% of the gas overlap ($2\sigma$); individual steps are weighted both by error ($1\sigma$ without $J$ error) and length (gas volume). Data reduction included standard corrections for interfering isotopes from nuclear interactions, extraction blanks, mass discrimination, and decay of $^{37}Ar$. Statistical analysis of the data and age calculations were done with the IAAA97 (Integrated Ar-Ar Analysis 1997, under development by T. H. Torsvik and coworkers, Geological Survey of Norway) software package for Windows 95. The heating schedule for feldspars followed Lovera et al. (1991). Feldspar diffusion and thermal modeling followed the programs of Lovera et al. (1989) and Lovera (1990), adapted to IAAA97. All feldspar samples were degassed at 270°–275°C for 2 h before analysis, to expunge surface contaminants. Other minerals were degassed for ca. 25 min at 350°C before analysis. Complete data tables and heating schedules for feldspars are reported in appendix A, available from *The Journal of Geology* free of charge upon request. Data for micas and amphibole are presented in table 1. Release spectra and sample tectonostratigraphic positions are presented in figure 2, inverse isochrons for micas and amphibole are presented in figure 3, and figure 4 shows laboratory and model diffusion data from feldspars.

***White Micas.*** The release spectrum for AS-2b white mica (NSD hanging-wall) yields a plateau with an age of 448 ± 2 Ma (77% of the total $^{39}Ar$; fig. 2), preceded by a group of increasing apparent ages over the first ca. 20% of $^{39}Ar$ released (see also Eide et al. 1997). The final two temperature steps represent <2% of the gas. The radiogenic nature of the samples precluded inverse isochron analysis. The plateau age is concordant with cooling ages obtained from numerous other Høyvik Group white micas from the island of Atløy and the mainland (Andersen et al. 1998). K/Ca and Cl/K ratios and petrographic examination indicate that the gas evolved from a fairly homogeneous, high-K white mica, in accord with results of Andersen et al. (1998).

The release spectrum for AS-6b white mica (detachment mylonite) yields a plateau with an age of 420 ± 2 Ma for 97% of the gas released (fig. 2). The radiogenic nature of the samples precluded inverse isochron analysis. Cl/K ratios indicate uniform Cl

**Table 1.** $^{40}Ar/^{39}Ar$ Data from White Micas, Biotite, and Amphibole, Western Norway

| Temperature (°C) | $^{40}Ar/^{39}Ar$ | $^{38}Ar/^{39}Ar$ | $^{37}Ar/^{39}Ar$ | $^{36}Ar/^{39}Ar$ ($10^{-3}$) | $^{39}Ar$ ($10^{-14}$moles) | $F^{39}Ar$[a] (cumulative) | $\%^{40}Ar^{\star}$[b] | $^{40}Ar^{\star}/^{39}Ar$ | Age (Ma) | $\pm 1\sigma$ |
|---|---|---|---|---|---|---|---|---|---|---|
| A. White mica (AS-2b):[c] | | | | | | | | | | |
| 700 | 34.615 | .086 | .074 | 9.222 | .25 | 3.28 | 91.68 | 31.86 | 352.09 | 5.71 |
| 800 | 39.514 | .028 | .011 | 2.643 | .24 | 6.43 | 97.64 | 38.72 | 419.72 | 5.44 |
| 850 | 40.908 | .021 | .002 | 1.769 | .68 | 15.31 | 98.58 | 40.38 | 435.64 | 6.58 |
| 900 | 41.690 | .021 | .000 | .906 | 1.69 | 37.53 | 99.30 | 41.42 | 445.59 | 6.63 |
| 950 | 42.098 | .021 | .000 | .626 | 1.80 | 61.18 | 99.51 | 41.91 | 450.27 | 6.44 |
| 1000 | 42.014 | .021 | .001 | .531 | 2.39 | 92.62 | 99.58 | 41.85 | 449.75 | 6.34 |
| 1100 | 43.529 | .022 | .019 | 2.934 | .44 | 98.39 | 97.79 | 42.65 | 457.32 | 6.59 |
| 1200 | 61.280 | .025 | .224 | 53.771 | .06 | 99.14 | 72.90 | 45.19 | 481.15 | 8.64 |
| 1400 | 141.747 | .095 | .057 | 378.955 | .07 | 100.00 | 19.71 | 28.07 | 313.63 | 33.2 |
| B. White mica (AS-6b):[d] | | | | | | | | | | |
| 700 | 36.500 | .027 | .046 | 3.991 | .29 | 2.61 | 93.66 | 35.35 | 383.48 | 6.51 |
| 800 | 38.489 | .023 | .010 | 1.371 | .16 | 4.06 | 92.82 | 38.09 | 410.09 | 7.67 |
| 850 | 39.467 | .023 | .006 | 1.902 | .53 | 8.88 | 96.61 | 38.92 | 418.00 | 6.79 |
| 900 | 39.802 | .023 | .003 | 1.480 | 2.37 | 30.45 | 98.45 | 39.37 | 422.37 | 6.15 |
| 950 | 39.602 | .023 | .003 | .711 | 4.09 | 67.74 | 99.19 | 39.40 | 422.60 | 5.91 |
| 1000 | 39.265 | .023 | .028 | .502 | 2.99 | 94.97 | 99.21 | 39.12 | 419.99 | 5.99 |
| 1050 | 39.497 | .023 | .105 | 1.650 | .42 | 98.80 | 95.74 | 39.04 | 419.14 | 6.18 |
| 1100 | 42.646 | .027 | .667 | 15.165 | .07 | 99.46 | 76.18 | 38.35 | 412.57 | 7.30 |
| 1200 | 63.043 | .042 | 1.299 | 111.249 | .03 | 99.77 | 38.11 | 30.97 | 340.18 | 12.69 |
| 1400 | 415.680 | .285 | .592 | 1394.640 | .03 | 100.00 | 2.55 | 11.31 | 131.77 | 106.46 |
| C. Biotite (T97):[e] | | | | | | | | | | |
| 600 | 39.690 | .039 | .011 | 111.962 | .14 | .52 | 18.10 | 7.18 | 228.92 | 5.68 |
| 650 | 21.224 | .025 | .008 | 34.080 | .75 | 3.20 | 53.26 | 11.30 | 348.17 | 9.10 |
| 700 | 15.712 | .020 | .005 | 11.441 | 1.36 | 8.09 | 78.65 | 12.36 | 377.41 | 8.22 |
| 750 | 14.367 | .019 | .004 | 5.915 | 1.13 | 12.15 | 87.80 | 12.61 | 384.48 | 8.19 |
| 800 | 13.809 | .019 | .003 | 3.327 | 1.36 | 17.03 | 92.75 | 12.81 | 389.78 | 7.96 |
| 850 | 13.391 | .018 | .002 | .907 | 4.74 | 34.06 | 97.76 | 13.09 | 397.53 | 8.46 |
| 900 | 13.293 | .018 | .002 | .797 | 4.02 | 48.51 | 97.98 | 13.03 | 395.72 | 8.18 |
| 950 | 13.678 | .019 | .005 | 1.742 | 2.53 | 57.60 | 96.04 | 13.14 | 398.75 | 10.62 |
| 1000 | 12.703 | .018 | .004 | 1.482 | 2.41 | 66.26 | 96.33 | 12.24 | 374.07 | 7.85 |
| 1100 | 12.931 | .018 | .002 | .713 | 7.28 | 92.41 | 98.11 | 12.69 | 386.46 | 7.96 |
| 1200 | 13.534 | .018 | .002 | .086 | 1.99 | 99.56 | 99.54 | 13.47 | 407.86 | 9.13 |
| 1400 | 63.975 | .048 | .000 | 179.281 | .12 | 100.00 | 18.67 | 11.95 | 366.04 | 64.78 |

**Table 1.** (*Continued*)

| Temperature (°C) | $^{40}Ar/^{39}Ar$ | $^{38}Ar/^{39}Ar$ | $^{37}Ar/^{39}Ar$ | $^{36}Ar/^{39}Ar$ ($10^{-3}$) | $^{39}Ar$ ($10^{-14}$moles) | $F^{39}Ar$[a] (cumulative) | $\%^{40}Ar^{\star}$[b] | $^{40}Ar^{\star}/^{39}Ar$ | Age (Ma) | $\pm 1\sigma$ |
|---|---|---|---|---|---|---|---|---|---|---|
| D. Amphibole (41A):[f] | | | | | | | | | | |
| 600 | 42.529 | .062 | 4.285 | 45.448 | .02 | .32 | 69.94 | 29.94 | 806.59 | 21.38 |
| 700 | 39.577 | .049 | 2.369 | 24.606 | .03 | .84 | 82.48 | 32.76 | 866.87 | 21.38 |
| 750 | 23.511 | .033 | 1.493 | 17.025 | .01 | 1.11 | 79.49 | 18.73 | 545.01 | 25.77 |
| 800 | 22.153 | .028 | 1.724 | 16.538 | .01 | 1.31 | 78.97 | 17.54 | 514.86 | 31.41 |
| 850 | 23.854 | .030 | 2.130 | 20.793 | .04 | 2.10 | 75.47 | 18.06 | 528.11 | 13.06 |
| 900 | 17.338 | .035 | 3.156 | 17.123 | .06 | 3.29 | 72.99 | 12.72 | 387.26 | 12.26 |
| 950 | 15.464 | .044 | 6.047 | 8.924 | .14 | 6.10 | 86.99 | 13.58 | 410.68 | 9.74 |
| 1000 | 13.954 | .034 | 10.007 | 5.442 | .56 | 17.52 | 95.69 | 13.56 | 410.18 | 9.06 |
| 1050 | 12.542 | .024 | 10.407 | 3.555 | 1.37 | 45.30 | 99.90 | 12.73 | 387.60 | 8.60 |
| 1100 | 12.646 | .021 | 9.497 | 3.140 | 1.43 | 74.31 | 100 | 12.84 | 390.79 | 8.83 |
| 1150 | 13.812 | .022 | 10.663 | 3.155 | .90 | 92.63 | 100 | 14.17 | 426.65 | 9.56 |
| 1200 | 13.948 | .022 | 10.925 | 3.564 | .28 | 98.41 | 100 | 14.22 | 427.99 | 13.31 |
| 1400 | 80.074 | .066 | 11.461 | 238.135 | .08 | 100.00 | 15.16 | 12.35 | 377.27 | 73.21 |

Note. Before irradiation, mineral fractions were packed in Sn-foil and irradiated at the Siloée reactor in Grenoble, France. Monitor minerals were the Fish Canyon Tuff feldspar (27.4 Ma) and the Caplongue hornblende (344.5 ± 0.5 Ma) (Cebula et al. 1986; Maluski 1996). Irradiation parameters (flux, salts, and shielding) were calculated after Arnaud et al. (1993). In addition to the double-vacuum resistance heating furnace (for feldspar analyses, table 2), we used a radio frequency furnace for white mica, biotite, and amphibole analyses. The latter furnace has regular temperature calibration by means of an optical pyrometer correlated to precise furnace power output. Temperatures for both furnaces are known at ±10°C for each step with 25-min step duration and 5-min gettering for all micas and amphibole. Interfering reactions on K, Ca, and Cl were determined by irradiation of pure salts together with the samples; variations in Cl/K ratios are monitored through the induced $^{38}Ar_{Cl}/^{39}Ar_{K}$ ratios. Because of the complexity of production of $^{38}Ar$ from nuclear interactions both on Ca and Cl, the direct calculation of elemental Cl/K values is semiqualitative since no precise multiplicative factor can be utilized to convert the isotopic to the element ratios.

[a] $F^{39}Ar$ = cumulative $^{39}Ar$ released.

[b] $40Ar^{*}$ = radiogenic $^{40}Ar$.

[c] Upper Plate; $J = 0.0067644$; weight = 1.2 mg.

[d] Upper Plate; $J = 0.0067000$; weight = 2.8 mg.

[e] Lower Plate; $J = 0.0188300$; weight = 2.93 mg.

[f] Lower Plate; $J = 0.0188300$; weight = 14.91 mg.

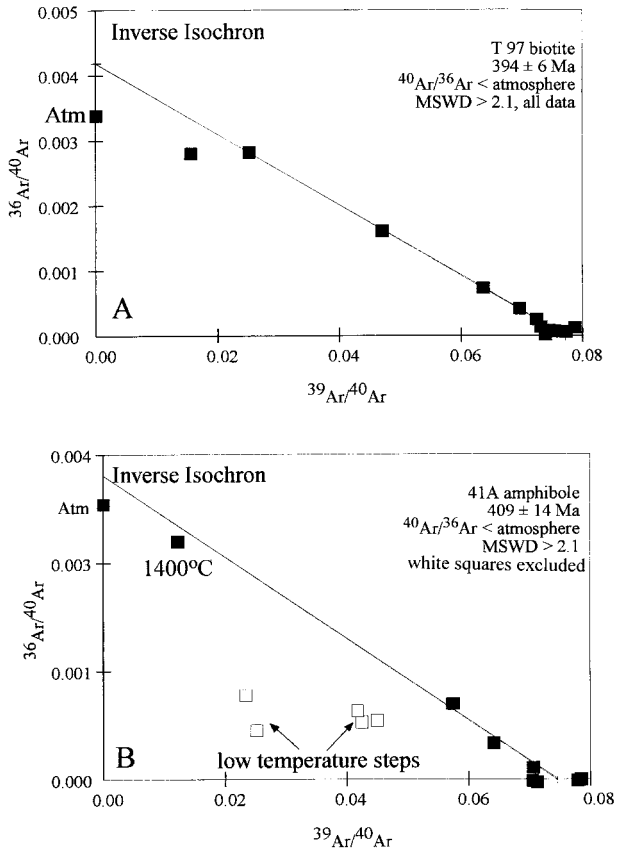


**Figure 3.** Inverse isochron diagrams for the biotite and amphibole samples from the WGR basement, corresponding to respective age spectra in figure 2 (*lower right corner*). *A*, Biotite from pegmatite filling a small shear zone yields a relatively poorly correlated fit of the data to a line with an intercept less than atmospheric value when all data are included. Utilizing only those data comprising the plateau age (fig. 2) yields an upper intercept of nearly atmospheric value but a worse correlation of the data to the line. The ordinate intercept of 394 ± 6 Ma is within uncertainty of the plateau age of 395 ± 2 Ma. The isochrons and consistency of the K/Ca and Cl/K ratios do not directly implicate any excess Ar. *B*, Barroisitic amphibole from a monomineralic vein filling an eclogite shows two clear data distributions. One distribution (*white boxes*) comprises a low-temperature series with Cl-correlated excess argon; the remaining higher-temperature steps define a mixing line (poorly correlated) between an atmospheric component of Ar and a radiogenic component with an age of 412 ± 2 Ma.

release for the plateau segment of the spectrum and slight Cl enrichment in the initial and final two low-volume temperature steps. Correspondingly, K/Ca ratios are very low in the initial and final temperature steps. While the K/Ca ratios are high and steady for most of the plateau segment, the decrease in K/Ca ratio in the highest-temperature step of the plateau may indicate some compositional inhomogeneity that otherwise has had no apparent influence on the relative proportions of $^{40}Ar^{\star}$ and $^{39}Ar$ released from the grain. The mica plateau age overlaps (at $2\sigma$) with the highest-temperature portion of the K-feldspar spectrum (AS-6a) analyzed from the same sample (see also "Alkali Feldspar $^{40}Ar/^{39}Ar$ Thermochronology").

***Biotite.*** Pegmatitic biotite (T97) from the shear zone in gneisses of the WGR yields a somewhat irregular spectrum, with apparent ages rising during the first 15% of gas released toward the plateau age of 395 ± 2 Ma (for 50% $^{39}Ar$ gas; fig. 2). The apparent age subsequently drops to 374 Ma and climbs in the remainder of the experiment to 408 Ma at fusion. Inverse isochron analysis yielded an array with reasonable spread between atmospheric and radiogenic components but a poor fit to the data, partly because of a high-temperature group of points with apparent excess argon. A poorly correlated line through all the data points yields an age of 394 ± 6 Ma with an $^{40}Ar/^{36}Ar$ ratio (impossibly) below atmospheric value (295.5; fig. 3*A*). The Cl/K ratios are low and constant. The K/Ca ratios were high but very variable, exhibiting a distinct drop between two "peaks"; this drop in K/Ca occurs at the same step where we observe a drop in the apparent age—off the plateau in the central portion of the experiment (table 1; fig. 2).

***Amphibole.*** Barroisitic amphibole (41A) from the eclogite fracture yields a slightly saddle-shaped spectrum, with apparent ages falling from unrealistically high values (807 Ma) to a saddle low of 387 Ma before climbing to an age of 426 Ma at fusion. The K/Ca and Cl/K ratios are very irregular and globally higher in the first five low-temperature steps; thereafter, these ratios are fairly constant through fusion. Inverse isochron analysis indicates that the five low-temperature high-Cl steps contain excess Ar (figs. 2, 3*B*). A fit of a line to the remaining data (constant K/Ca and Cl/K ratios) yields a poorly correlated line corresponding to an age of 409 ± 14 Ma with an unrealistic abcissa intercept lower than (but statistically overlapping) atmospheric value (fig. 3*B*). On the spectrum plot, the eight highest temperature increments (also those used in the isochron diagram) yield a weighted age of 412 ± 2 Ma (fig. 2).

***Mica and Amphibole Data Interpretation.*** The white micas AS-2b and AS-6b represent homogeneous micas that cooled through ca. 350°C–400°C at 448 Ma (AS-2b) and 420 Ma (AS-6b). This temperature range has been suggested for white micas for cooling rates of a few tens of degrees per million

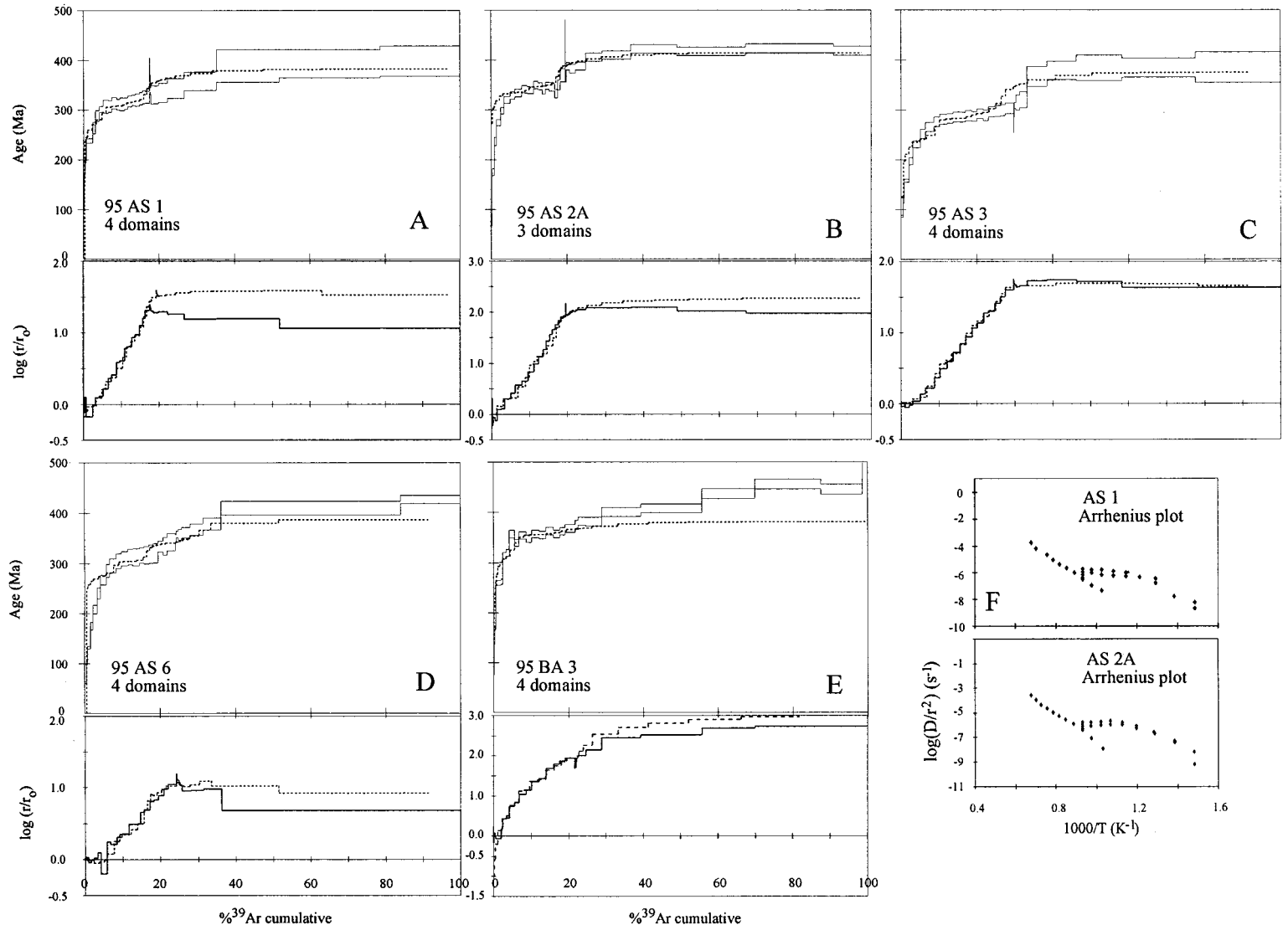
95 AS 1
4 domains
A
95 AS 2A
3 domains
B
95 AS 3
4 domains
C
95 AS 6
4 domains
D
95 BA 3
4 domains
E
Age (Ma)
log (r/r$_o$)
%$^{39}$Ar cumulative
AS 1
Arrhenius plot
F
AS 2A
Arrhenius plot
log(D/r$^2$) (s$^{-1}$)
1000/T (K$^{-1}$)

years (e.g., Hames and Bowring 1994) and coincides broadly with both the >400°C temperatures suggested by the analysis of some ductile deformation textures in the area (Chauvet and Séranne 1989; Andersen et al. 1998) and a 360°–370°C minimum suggested by the feldspar modeling results (see "Alkali Feldspar $^{40}Ar/^{39}Ar$ Thermochronology" and table 2). We note that temperatures derived from alkali feldspar MDD analyses are not uniquely constrained. The 448-Ma age for AS-2b is interpreted to be a "cooling age," achieved during rapid exhumation of the rocks subsequent to a Late Ordovician thermal event before the main Scandian phase of the Caledonian cycle (Andersen et al. 1998).

Sample AS-6 derives from a thick, highly sheared, ductile mylonite with fabrics indicating clear top-west shear sense. The most likely explanation for the 420-Ma age of AS-6b white mica is that of cooling through ca. 350°–400°C during the postcontractional extension. The pervasive top-west fabric in the mylonites and much of the basement in western Norway (Chauvet and Séranne 1989; Andersen and Jamtveit 1990; Fossen and Dunlap 1998) and the relatively high temperatures expected for formation of these strongly recrystallized rocks support this interpretation. This latest Early Silurian cooling age implies early initiation of extension in this particular area, relative to cooling ages from other studies elsewhere in western Norway (e.g., Berry et al. 1995; Fossen and Dunlap 1998) and would imply that some of the extension must have closely followed on and probably overlapped with the earliest phases of collision between Baltica and Laurentia. Two alternative, but to us less supportable, explanations for this age are that (1) the sample incorporated some unknown, uniformly distributed quantity of excess argon or (2) the sample somehow maintained relict argon from the contractional (top-east) phase of deformation. We would suggest that the high temperatures (>400°C) for plastic deformation and the complete recrystallization of minerals to define only top-west fabrics preclude the second explanation. While the data do not allow reasonable assessment of a "uniform excess argon component," we would note that feldspars in the sample would also need to have taken up the excess argon from a uniform reservoir in the same manner to account for the statistically similar 419-Ma age in the upper temperature steps of feldspar AS-6a (see also "Alkali Feldspar $^{40}Ar/^{39}Ar$ Thermochronology"). We cannot exclude excess argon as a possibility but favor the explanation that these ages are geologically significant to the timing of some extension in the mylonite.

The biotite release spectrum and K/Ca ratios (T97; figs. 2, 3*A*) indicate argon released from a chemically inhomogeneous and/or disturbed biotite. While the basis for this inhomogeneity is unknown, the coarse, euhedral, and undeformed appearance and lack of Cl-related contamination in the large biotite crystals in this pegmatite do not suggest significant recrystallization or alteration subsequent to pegmatite emplacement. While slightly uneven degassing of biotites under high vacuum (e.g., Gaber et al. 1988) might be invoked to explain the irregular argon release, we interpret the plateau age of 395 ± 2 Ma as closely approximating the cooling age for these biotites through closure temperatures between ca. 300° and 350°C (McDougall and Harrison 1988) shortly following emplacement of the pegmatite.

The age spectrum for the amphibole fracture filling (41A) is likewise disturbed. The very high ages in the early part of the spectrum are certainly attributable to Cl-correlated excess Ar (fig. 3*B*). The weighted age of 412 ± 2 Ma obtained from the remaining steps with stable K/Ca and Cl/K ratios is interpreted only as a maximum age for the cooling of the minerals since the slight saddle shape of the spectrum and isochron analysis indicate complications from excess argon. This cooling age must represent closure to argon below temperatures of ca. 450°–500°C, the interpreted maximum range for retrograde amphibolite facies conditions experienced by the eclogite facies rocks. The excess argon may have been derived directly from the surrounding eclogite body during depressurization and/or

**Figure 4.** Age spectra and modeling results for alkali feldspars from the profile. *A–E*, Upper diagram in each figure is the laboratory release spectrum (duplicated from fig. 2) and the corresponding "best-fit" modeled spectrum (*dotted line*), with the lower diagram comprising the laboratory $\log(r/r_o)$ versus $^{39}Ar$ cumulative plot for each sample (*solid line*) and the corresponding model curve (*dashed line*). The number of diffusion domains used in the modeling is also indicated for each sample. *F*, Two examples of Arrhenius plots from the sample set; all Arrhenius plots had basically similar data values and distributions. In *A–E*, we note that the high-temperature portions of the experiments were very difficult to model because of the breakdown (melting) of the feldspar above furnace temperatures of ca. 1140°C. We thus focused on model fits to the lower-temperature sections of the spectra.

**Table 2.** Alkali Feldspar Diffusion Parameters and Modeling Results

| Sample and domain | *E* (kcal/mol) | Frequency factor (1/sec) | Volume fraction (%) | Cooling rate (°C/m.yr.) | Temperature (°C) |
|---|---|---|---|---|---|
| AS-1: | | | | | |
| 1 | 35 | 6 | 3 | 1.7 | 123 |
| 2 | 37 | 5.4 | 6 | 50.0 | 159 |
| 3 | 40 | 4.8 | 6 | 30.0 | 201 |
| 4 | 49 | 3.2 | 85 | .6 | 366 |
| AS-2: | | | | | |
| 1 | 36 | 5.5 | 8 | .9 | 143 |
| 2 | 40 | 4.8 | 8 | 40.0 | 199 |
| 3 | 50 | 3.3 | 84 | 1.8 | 371 |
| AS-3: | | | | | |
| 1 | 36 | 6.3 | 7 | .4 | 126 |
| 2 | 38 | 5.4 | 8 | 20.0 | 167 |
| 3 | 40 | 4.6 | 8 | 30.0 | 210 |
| 4 | 49 | 3.6 | 77 | 1.0 | 348 |
| 95 AS-6a: | | | | | |
| 1 | 35 | 5.9 | 6 | .8 | 123 |
| 2 | 38 | 5.1 | 9 | 15.0 | 174 |
| 3 | 45 | 4.5 | 9 | 2.1 | 268 |
| 4 | 50 | 3.2 | 76 | 1.5 | 375 |
| 95 BA 3: | | | | | |
| 1 | 35 | 4.8 | 3 | .5 | 143 |
| 2 | 37 | 4.0 | 11 | 8.0 | 192 |
| 3 | 48 | 5.0 | 5 | 20.0 | 287 |
| 4 | 51 | 3.67 | 81 | 2.2 | 367 |

Note. Results from diffusion and thermal modeling runs include *E* (activation energy), frequency factor, cooling rate, and temperature at the start of each cooling "period." The diffusion parameters derived for each domain after numerous iterations yield synthetic fits in figure 4 and cooling curves of figure 5. The largest gas-volume domain 4 (or 3 for AS-2) had *E* between 49 and 50 kcal/mol. The *E*'s for these high-temperature domains are within the ranges suggested for single-domain, high-purity orthoclase feldspars (Foland 1974; Arnaud and Kelley 1997), and for many other K-feldspars from a variety of rock types and geologic settings (Lovera et al. 1997).

dewatering of the surrounding gneisses during exhumation; any compositional redistribution of potassium in these very low-potassium amphiboles, not unlikely during retrogression from amphibolite facies, may also have influenced the irregular distribution of argon in the mineral.

## Alkali Feldspar $^{40}Ar/^{39}Ar$ Thermochronology

***Data.*** The release spectra, Cl/K ratios, and Arrhenius plots from cycled, isothermal heating experiments from the five feldspar samples have very similar patterns, albeit with some intersample age variations at specific sections of the heating schedules (figs. 2, 4; app. A). The basic release spectrum patterns in figure 2 define (1) a set of low-temperature, low-volume steps (<8% of $^{39}Ar$ gas) with ages that rise rapidly from <100 Ma to (2) a tightly clustered, semiconcordant, or slightly increasing group of ages that range from 290 to 360 Ma and make up 12%–20% of the total gas, with a fairly abrupt transition to (3) a group of high-temperature, high-volume (60%–80% of the gas total) steps usually defining Early-Middle Devonian plateau ages. Individual steps corresponding to the middle group of broadly "Carboniferous" ages comprise relatively small gas volumes elicited during the isothermal portion of the furnace heating experiments. We draw attention also to the concave-downward cusp that is characteristic of the change from the low-temperature, rapidly rising age group to the semiconcordant, "Carboniferous" age group (fig. 2).

The Cl/K ratios are typically very high in the first two low-temperature steps of the feldspar analyses and fall to variable, but low, values for the remainder of the isothermal portion of each experiment; these values vary subtly in the high-temperature sections of the experiments (app. 1). On Arrhenius diagrams, the data define three different groups: the low- and high-temperature groups have broadly similar, subparallel negative slopes, separated by the middle group of steps defining a subhorizontal line with $\log(D_0/r^2)$ values ranging from $-5$ to $-6$ (fig. 4*F*).

The feldspar release spectrum from the structurally highest sample, AS-2a (Høyvik Group; phengite from the same rock = 448 Ma; see "White Micas"), climbs from an apparent age of 79 Ma to 298 Ma within the first 3.4% of $^{39}Ar$ gas released (fig.

2). The middle group of semiconcordant ages ranges from 298 to 350 Ma. In the upper part of the monotonically increasing portion of the heating schedule, the apparent ages reach a semiplateau of 419 ± 2 Ma that makes up 70.8% of the $^{39}$Ar gas.

Apparent ages from feldspar AS-1 (Dalsfjord Suite, structurally below AS-2; fig. 2) climb from 101 Ma to 289 Ma within the first 4.1% of $^{39}$Ar released. A group of semiconcordant ages (isothermal steps) then rise gradually to 326 Ma. At the shift to the monotonic temperature schedule, ages rise again to reach a plateau in the high-temperature/fusion portion of the experiment with an integrated age of 384 ± 4 Ma (73.4% of the gas volume).

The release spectrum from the structurally lower Dalsfjord Suite sample, AS-3, has a pattern shape nearly identical to AS-1, except that all apparent ages are offset to lower values. The ages climb from 86 Ma to 276 Ma during the first 2.5% of $^{39}$Ar released. The remaining isothermal temperature steps define a group of semiconcordant ages that rise gradually to 320 Ma. The final, high-temperature part of the experiment yields a plateau at 381 ± 2 Ma for 66.7% of the gas volume (fig. 2).

Feldspar from the mylonite (AS-6a) yields a release pattern representing broadly four definable segments. Initial ages rise rapidly from 61 to 267 Ma (5.8% of the evolved gas) and reach a group of semiconcordant steps ranging from 286 to 320 Ma (13.7% of gas). The final isothermal steps (three steps at 800°C) and the subsequent five cycled, monotonically increasing steps define a slightly more sharply rising group of ages from 334 to 379 Ma over 16.7% of the experiment. The majority of gas is released in two steps during final melting and fusion and gives a simple mean age of 419 ± 2 Ma (63.8% of the gas); note the similarity of this age to the plateau age (420 Ma) of white mica AS-6b from the same sample (fig. 2 and "White Micas").

The early part of the release spectrum for sample BA-3 (HP gneissic basement) exhibits rising ages grouped in low-volume, semiplateau pairs at 93 and 260 Ma and comprising 2.4% of the evolved gas (fig. 2). The gas-release theme common to the other feldspars is repeated during the bulk of the isothermal steps that define a group of semiconcordant steps ranging in age from 347 to 376 Ma (ca. 17% of the gas). The final 80% of the gas released in the high-temperature portion of the experiment yields discordant ages rising from 382 Ma to an unrealistic 636 Ma at fusion.

***Modeling Results and Interpretation.*** In the modeling exercises, Ar diffusion was assumed to follow the Arrhenius relationship $D = D_o \exp^{-E/RT}$ in feldspars comprising several diffusion domains of differing sizes and activation energies (Dodson 1973; Lovera et al. 1989; Harrison et al. 1991), where $D$ is the diffusion coefficient with a value equal to $D_o$ as absolute temperature approaches infinity, $R$ is the gas constant, and $E$ is the activation energy. "Domain" is essentially used in this discussion to describe the reservoirs from which argon was derived in the samples. We followed the modeling procedure described in Lovera et al. (1991) and assumed a plane slab geometry throughout the exercises. To obtain the diffusion parameters for each domain, we generated first, synthetic Arrhenius plots to compare to the laboratory Arrhenius plots. For these initial runs, the number of domains and the domain volume fraction were based on visual evaluation of the release spectra, while initial $E$ and frequency factors were determined by the slope and intercept of a line through the low-temperature leg of the laboratory Arrhenius distribution (see, e.g., fig. 4*F*). Frequency factors and $E$ for the other domains were revised in iterative fashion in subsequent runs after visual evaluation of the model fit to the data. We were able to model all the feldspars reasonably by using either three or four diffusion domains; slightly better fits were arguably achieved in a few samples where we utilized a larger number of domains, although the cooling histories generated are not sensitive to the number of diffusion domains used in the modeling exercises.

Once an acceptable visual fit to the Arrhenius diagram was achieved, the diffusion data were plotted on the log $(r/r_o)$ plot; this representation of the model data is insensitive to the heating schedule of the experiment (Richter et al. 1991) and thus provides the most independent means to assess the fit of the modeled argon diffusion parameters to the laboratory diffusion data (Lovera et al. 1991). The log $(r/r_o)$ plots illustrate the change in effective diffusion length scale $(r)$ versus a reference scale $(r_o)$ during the experiment (%$^{39}$Ar released); in this manner it is possible to evaluate the relative sizes of the domains as the experiment progresses. In our modeling, obvious misfits between the laboratory and the synthetic log $(r/r_o)$ data were addressed iteratively. The accepted fits are presented in figure 4*A–E*. For reasons discussed below, misfits of the synthetic models to the highest temperature portions of the log $(r/r_o)$ plots were given less priority than achieving acceptable fits in the lower-temperature portions of the experiments.

Finally, diffusion parameters from the "best-fit" log $(r/r_o)$ plots were used to calculate thermal histories for each domain in the sample. We utilized the cooling age and (assumed) closure temperature

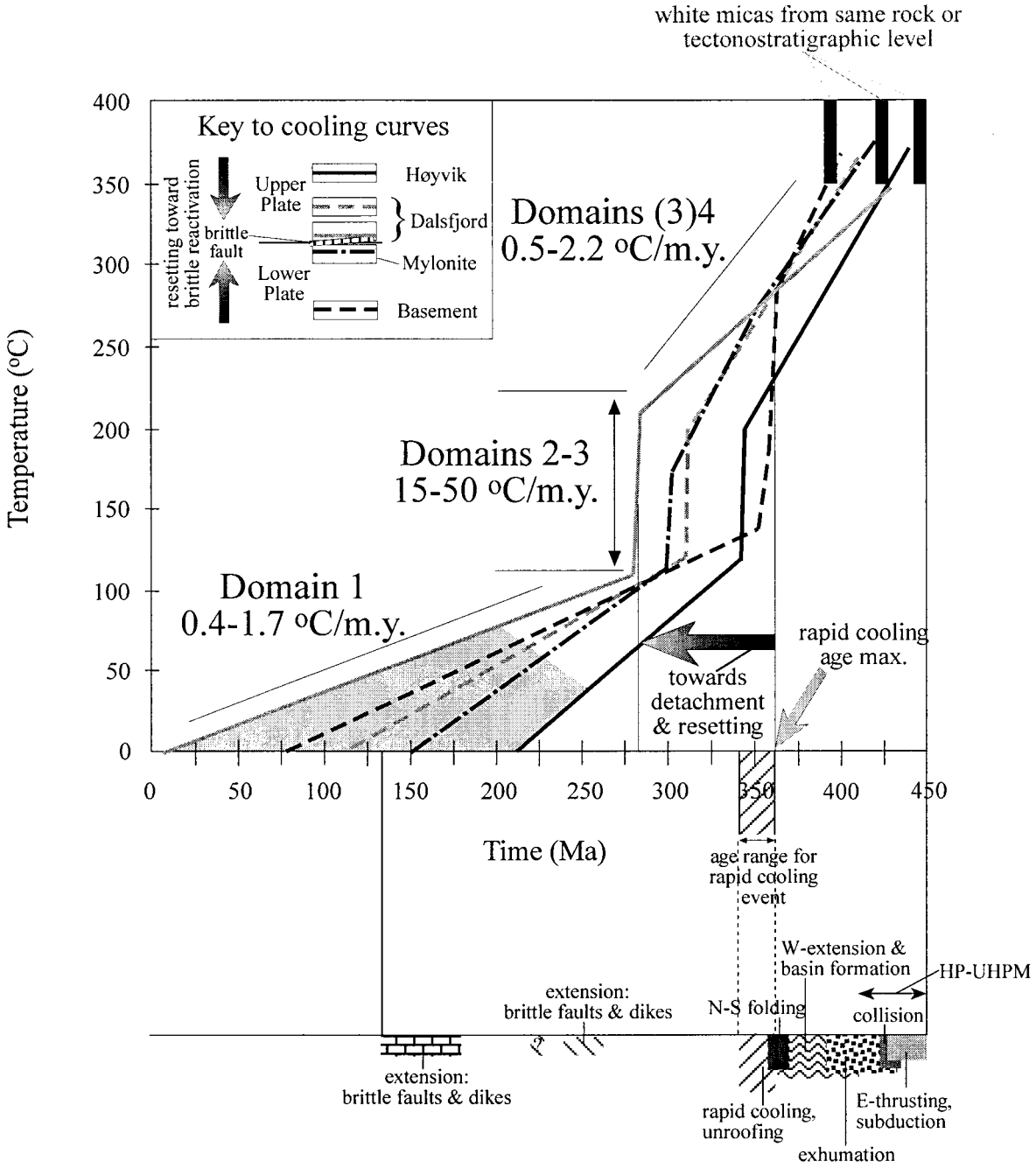


**Figure 5.** Cooling curves generated by data derived from modeling in figure 4 and displayed in table 2. Coding in upper left corner of the graph is a schematic representation of the tectonostratigraphic levels for corresponding feldspar cooling curves. We note the "starting" points in the runs (control from white mica ages from three rocks where feldspars were also analyzed). The upper-temperature, more retentive domains (domains 3 and 4) are best modeled via slow cooling (0.5°–2.2°C/m.yr.) from the time of blocking of white micas below ca. 400°C. All feldspars subsequently exhibit the same very dramatic break in slope, albeit at slightly different times, that corresponds to very rapid cooling of the feldspars (at rates >15°C/m.yr.; domains 2 and 3). The rapid cooling episodes are followed by another period of slow cooling (0.4°–1.7°C/m.yr.) and/or partial Ar-loss until the rocks reached surface levels (domain 1). The lower portion of domain 1 is shaded in gray where the geologic meaning

of the white micas analyzed in this study for the initial (upper) boundary conditions of the thermal modeling runs and selected cooling rates and starting temperatures for each domain in the sample (table 2). The cooling histories generated from these inputs were then evaluated by generating a synthetic age spectrum from the model cooling history and comparing this result to the observed age spectrum (fig. 4*A–E*). Misfits to the laboratory spectrum were addressed iteratively until a visually acceptable match between synthetic and laboratory spectra was obtained.

Domain 1 in all the feldspars corresponds to the lowest-temperature portion of the heating experiments, represented on the release spectra by the group of rapidly increasing, small gas-volume temperature steps (figs. 2, 4, 5). Domains 2 and 3 correspond to the bulk of the isothermal heating steps, represented on the release spectra by the group of tightly clustered, semiconcordant data yielding broadly "Carboniferous" ages. Domain 4 (or 3 in sample AS-2) corresponds to the high-temperature, large gas-volume steps that generally yield the late Silurian to Early-Middle Devonian plateau ages.

Table 2 lists activation energies, frequency factors, volume fractions, and the thermal modeling results from our analyses of the five feldspars. We utilized different activation energies for the various domains, although our modeling runs using a single activation energy reproduced very well the shapes of the cooling curves generated with different activation energies. This nonuniqueness of the activation energies in the MDD analysis affects the temperatures for each domain but not the shapes of the paths themselves, which should be very specific to the thermal histories of the individual feldspar samples. Clearly, the high-volume, high-temperature domains tended to dominate the model fits to both Arrhenius and age spectra plots; however, since the volume diffusion properties of Ar in feldspar are not valid above melting temperatures (about 1140°C in the furnace; Lovera et al. 1991; Richter et al. 1991; Arnaud et al. 1993), we deprioritized poor fits in the upper portions of the log ($r/r_o$) plots in instances where forcing a fit to those high-temperature data compromised fits in the lower-temperature portions of the heating experiments (fig. 4*A–E*).

The modeled cooling histories were very similar for each of the feldspar samples (fig. 5), whereby domains 1 and 4 (or 3) achieved best fits with slow cooling rates: 0.4°–1.7°C/m.yr. for domain 1 and 0.6°–2.2°C/m.yr. for domain 4 (or 3; figs. 4, 5; table 2). The middle domains 2 and 3 fit the observed data only when rapid cooling rates were applied. We found generally that all fits for domains 2 and 3 were better at cooling rates above 15°C/m.yr.; the fits for several of the samples (AS-1, AS-2, and AS-3) were better when rates between 20° and 50°C/m.yr. were used (table 2; 4). The model fits did not improve greatly, nor did they collapse, when rates up to 100°C/m.yr. were used. However, because of ongoing discussion related to the realistic ability to utilize and assess cooling rates and paleogeotherms (e.g., Manckelow and Grasemann 1997), we allocate the more conservative, minimum rate of 15°C/m.yr. for domains 2 and 3; this value is nonetheless an order of magnitude higher than that recorded by the feldspars either during domain 1 or 3 cooling segments. We underline the fact that it is the shape of the cooling curve, and not the actual temperature represented at each interval/segment, that is unique for each feldspar; thus, the strength of our modeling results lie in the fact that feldspars from very different rock types have yielded cooling paths with very similar shapes.

In figure 5, the onset of the rapid cooling episode in each of the feldspars, represented by domains 2

---

of the modeling results becomes more speculative and the ability to model the feldspar data more difficult. Inspection of the age differences at the onset of the rapid cooling episode (start of domains 2 and 3) reveals that the two "oldest" rapid cooling episodes (*black*, *solid*, and *dashed lines*) correspond to the uppermost (Høyvik Group, *solid*) and lowermost (basement, *dashed*) feldspar samples in the profile. Map locations in figure 1*b* show that these samples are geographically and stratigraphically farthest from the NSDZ. The "youngest" apparent onset of rapid cooling corresponds to the feldspar sampled within the detachment mylonite (*gray solid curve*) and is very close to brittle faults with known ages of activity in the Late Permian and Late Jurassic (see Torsvik et al. 1992; Eide et al. 1997). We thus interpret these apparent differences in age of onset of the rapid cooling event to represent different degrees of postcooling resetting in Late Permian and/or Mesozoic times as the NSDZ was episodically reactivated (Osmundsen et al. 1998). The samples farthest from the detachment were not reset and thus represent most accurately the timing of onset of the rapid cooling episode (i.e., between 340 and 360 Ma). The lower part of the figure places the Paleozoic through Mesozoic events in chronological order and emphasizes the overlapping nature of subduction, thrusting, collision, exhumation, and extensional processes.

and 3, occurs at a slightly different time period. Those feldspars located structurally (tectonostratigraphically) farthest from the Atløy brittle fault yield the oldest ages for onset of the rapid cooling event (340–360 Ma), while those closest to the fault yield the youngest ages (as low as ca. 280 Ma). We suggest that this difference does not necessarily represent real differences in the age of onset of this rapid cooling "event" but, rather, can be attributed to partial resetting of the Ar systems in those rocks closest to the reactivated fault. The Atløy brittle fault was reactivated at least twice, in the Late Permian and latest Jurassic–Early Cretaceous; fluid flow and recrystallization of new fault minerals occurred during both phases (Torsvik et al. 1992; Eide et al. 1997). We suggest that the HP basement (BA-3) and the allochthonous Høyvik Group (AS-2a) feldspars, in the tectonostratigraphically lowest and highest positions in our profile, respectively, were isolated from the fluids and/or frictional heating associated with these younger fault reactivation/resetting events. These two samples, with very similar ages for the onset of rapid cooling, thus record most accurately the time of the event—that is, in the Late Devonian–Early Carboniferous, between 340 and 360 Ma (fig. 5). Ongoing work demonstrates that the physical crushing activity and fluid circulation at the time of brittle faulting caused argon loss in feldspars analyzed from directly within the brittle fault rocks (Arnaud and Eide 1998).

## Discussion

What geologic significance can we place on the argon reservoirs in each of these feldspar samples, given that similar cooling histories are produced in feldspars from very different rocks with different degrees of deformation? First, the high-temperature domain (domains 3 and 4) corresponds to very retentive sites for argon in the feldspar structure; these sites are characterized by high-K and low-Cl contents and apparent ages that are in keeping with cooling after Caledonian-related tectonic activity, during the rocks' exhumation. This interpretation is strengthened by the very good correspondence to plateau ages from the samples where white micas were also analyzed.

In sample AS-2, from the nappe unit, the 448-Ma white mica age and the 420-Ma high-temperature plateau age from domain 3 of the feldspar imply relatively slow cooling from assumed closure temperatures of ca. 400° and 370°C, respectively (ca. 1°C/m.yr.). That these rocks remained at shallow crustal levels during Scandian (ca. 430–410 Ma), eastward nappe emplacement has been documented previously (Andersen et al. 1998).

The high-temperature, domain 4 plateau ages for samples AS-1 and AS-3, both from the Dalsfjord Suite mangerite in the lowermost part of the nappe unit (fig. 2), are younger (384 and 382 Ma, respectively) than those for the stratigraphically higher AS-2a. The two mangerite feldspars appear to have undergone the same Middle Devonian cooling through approximately similar closure temperatures (see table 2). The cooling age difference (40 m.yr.) between the feldspars in the Dalsfjord Suite and that in the tectonostratigraphically higher Høyvik Group (AS-2a) is attributed to stronger Caledonian (Scandian phase) deformation and heating in the mangerite samples; the Dalsfjord rocks directly overlie the décollement surface over which the nappes were first thrust eastward and subsequently extended westward.

In sample AS-6, from the mylonite, where we also have both white mica and feldspar data, the high-temperature plateau (419 Ma) of the feldspar overlaps within uncertainty the plateau age of the mica (420 Ma; see fig. 2), implying crystallization of the mica and closure of domain 4 in the feldspar in the mylonite zone, probably at similar temperatures. We would infer that the closure temperature of the white mica was slightly higher than that of domain 4, but the modeling does not uniquely control this parameter. For reasons discussed previously, we interpret the 420-Ma age to document cooling during early westward movement on the extensional detachment, although excess argon complications cannot be completely excluded. We make note that the present geographic proximity of sample AS-6 (mylonite) to mangerite sample AS-3 is an artefact of the westward extension; at 420 Ma, the nappe units lay at least 100 km to the east of their present location.

Deeper into the basement, sample BA-3, the slightly irregular, climbing steps of the high-temperature portion of the experiment correspond to domain 4. These steps do not yield a statistical plateau, but one segment of the upper temperature series has consecutive steps corresponding to ages of ca. 400 Ma, comparable to numerous mica cooling ages from elsewhere in the basement of ca. 395–405 Ma (see Berry et al. 1995; Boundy et al. 1996; Fossen and Dunlap 1998; this study). The higher temperature set of climbing ages (420 to 636 Ma at fusion) cannot be convincingly interpreted to represent any geologically relevant event; all available geochronologic and metamorphic pressure-temperature information demonstrates that basement rocks in western Norway, now preserved

**Table 3.** Calculated Estimates of Unroofing Rate and Upward Distance Traveled by the Two End-Member Western Norway Rocks (Samples BA-3 and AS-2) during the Rapid Cooling Episode for a Specified Constant Geotherm

| Geothermal gradient (°C/km) | Duration of cooling (m.yr.) | | Temperature cooled during interval (°C) | | Calculated upward movement in the time interval (km) | | Smoothed unroofing rate (mm/yr) | |
|---|---|---|---|---|---|---|---|---|
| | BA-3 | AS-2 | BA-3 | AS-2 | BA-3 | AS-2 | BA-3 | AS-2 |
| 10 | 5 | 2 | 95 | 50 | 9.5 | 5.0 | 1.9 | 2.5 |
| 15 | 5 | 2 | 95 | 50 | 6.3 | 3.3 | 1.3 | 1.7 |
| 20 | 5 | 2 | 95 | 50 | 4.8 | 2.5 | 1.0 | 1.3 |
| 25 | 5 | 2 | 95 | 50 | 3.8 | 2.0 | .8 | 1.0 |

at eclogite facies, reached temperatures of at least 550°C during the Scandian collision (430–410 Ma), thus mandating complete outgassing of argon in any of the basement feldspars or micas in the region. These "old" ages are probably related to some excess argon component, trapped in the highly retentive sites of the feldspar directly after HP metamorphism.

Domain 1, corresponding to the lower gas-release temperatures, was more difficult to model because of the small volume of gas it represents in all the feldspars analyzed. The rapidly decreasing ages in this segment of all the feldspar experiments are caused by a combination of factors: geologic exhumation/cooling, partial resetting, and release of the argon in the laboratory from generally less retentive sites in the grain surfaces. Some of these less retentive sites would include fluid inclusions (especially for Cl-correlated steps), cracks, and subgrains and other strain-induced features (especially those samples taken in close proximity to the fault zone). The young, brittle extensional events for which we have both on- and offshore documentation (Late Permian and Late Jurassic–Early Cretaceous; Torsvik et al. 1992; Færseth 1996), are directly monitored by feldspars from the Atløy fault rock. However, farther from the fault, the heat or uplift associated with faulting activity was not marked enough to be precisely monitored by feldspars outside the fault zone (Arnaud and Eide 1998). Regional apatite fission track studies in southern Norway (Rohrman et al. 1995) have documented regional uplift of southern Norway in the Triassic and Jurassic, as well as in Neogene times, so some low-temperature disturbance of the low-volume, low-retentivity domains in the feldspars would be anticipated. Because of this varied combination of influences on the low-temperature portion of our MDD feldspar modeling, we have placed the lowermost (youngest) part of the cooling curves in figure 5 in gray shading to indicate uncertainty with the shape of this part of the path.

The nature of domains 2 and 3, which yield the rapid cooling signatures (fig. 5), is more speculative, and we can only propose that these represent some original part of the feldspar lattice that remained open to diffusion of radiogenic argon until Early Carboniferous times. We reason that the middle domain is a potassium-related site and not an anion site from the fact that the same release patterns and relative proportions of radiogenic and reactor-induced argon are produced from different samples.

A minimum calculation of an exhumation rate for these rocks during this rapid cooling episode mandates knowledge of three parameters: (1) starting/ending temperatures of the "episode" for the rocks in question, (2) the cooling rate, and (3) the geothermal gradient. We know parameters 1 and 2 but have no real control on 3. However, if we assume a steady-state geothermal gradient over the duration of the cooling "event" (1–5 m.yr.), an assumption perhaps warranted by the brief duration of the rapid cooling period and by the fact that the rocks were relatively close to the earth's surface (see Manckeltow and Grasemann 1997), we can make minimum calculations for vertical movement (exhumation) of these rocks. For the two end-members apparently unaffected by Permian and/or Mesozoic reactivation events (AS-2 and BA-3), table 3 shows that for a broad range of steady state geotherms, the rocks may have been exhumed between 2 and 4 km. The actual vertical (structural) distance between these two rock units in the tectonostratigraphic package for that time period is impossible to reconstruct accurately, but this would probably translate to ca. 500 m of acutal "uplift." Implicit in our discussion is the fact that, although the "cooling event" was latest Devonian (Famennian)–Early Carboniferous in age, the actual rapid upward movement of the rocks must have begun

slightly earlier (Givetian? Frasnian?) because of the inherent lag of a thermal response to an exhumation episode (see, e.g., Manckeltow and Grasemann 1997).

## Regional Significance

Two simple explanations for a rapid cooling event can be proposed: (1) a cooling response from a thermal pulse caused by magma intrusion or (2) a response to exhumation from a warm to a relatively cooler crustal level (because of tectonic and erosional processes). Our modeling of these feldspars did not take into account any possibility of episodic thermal pulses: in western Baltica, we lack any evidence for enhanced syn- or postcollisional magmatic activity. We thus favor the second, tectonic/erosion unroofing situation for the western Norway region; however, we note that the unroofing may have been induced by thermal underplating that never achieved surface expression in the form of igneous products.

The approach of a crustal unit toward the earth's surface can be accomplished by tectonic exhumation, fault-controlled footwall uplift accompanied by increased rates of erosion, or, more generally, increased topography and erosion. We briefly examine each of the three mechanisms.

The rocks in this area underwent "tectonic exhumation" during and immediately after continental collision in Early-Middle Devonian time, as demonstrated by a variety of structural, kinematic, and geochronologic data (see Andersen 1998; Fossen and Dunlap 1998). By the Early Carboniferous, the geologic evidence in western Norway implies that this postcollision, exhumation period was completed (Osmundsen et al. 1998) and thus sudden "unroofing" in the area during Early Carboniferous time must have a different, but not necessarily unrelated, cause.

Fault-controlled footwall uplift is sometimes necessitated in sedimentary basin modeling to clarify abrupt changes in basin thermal and stratigraphic histories. In the case of western Norway, some form of footwall uplift in the Early Carboniferous would have required a regional normal fault or fault system. First, the Caledonian detachment system by this time had been cross-cut and bypassed by several other fault splays and systems, especially with respect to formation of the Early-Middle Devonian basins (Osmundsen et al. 1998); thus, the function of the NSDZ as a sole controlling factor affecting uplift of the entire Sunnfjord region in latest Devonian–Early Carboniferous time is remote. Furthermore, both hanging walls and footwalls in the detachment system display the rapid-cooling signature. Presently, only the Øygarden Fault Zone (ØFZ; fig. 1) emerges as a candidate to affect the sort of crustal movement required for "footwall uplift"–related cooling. Based on current estimates of depth-to-basement on both sides of the fault zone, interpretations of the ØFZ geometries (seismics), and estimates of apparent ages/thicknesses of sedimentary packages on the western side of the fault (P. Osmundsen, personal communication), activity/initiation of the ØFZ in Early Carboniferous time is unlikely. We argue below that the rapid cooling recorded in these rocks was rooted much more fundamentally and regionally and implicates increased topography and erosion to account for the rapid cooling recorded in these rocks.

Increased topography in this area may be caused by regional thermal underplating. In the case of western Norway, this increased topography was probably accompanied by or immediately postdated regional folding and low-grade metamorphism (along east-west axes) of both the detachment and the basal sediments in the Devonian basins of western Norway (see "Introduction" for details). The timing of our independently derived Early Carboniferous cooling event coincides well with relative time constraints previously suggested for this folding episode and, in fact, recalls the "Solundian and Svalbardian" orogenies proposed for this and other areas of the Late Devonian North Atlantic margin (see Harland et al. 1984; Torsvik et al. 1986; Krabbendam and Dewey 1998; Osmundsen et al. 1998). However, if folding in western Norway can indeed be pinpointed to latest Devonian–Early Carboniferous times, it must also (in western Norway) have been accompanied by regional unroofing. Obviously, folding alone cannot accomplish the cooling response we observe in the rocks since fold geometries predict variable cooling rates depending on a rock's position within the fold sequence. Increased topography must lie behind the thermal response that we observe in the feldspars; if caused by thermal underplating, we would not necessarily expect to see extensive melting and magma production, primarily because the lithosphere in western Norway (western Baltica) was, and has remained, quite thick (see, e.g., Hurich and Kristoffersen 1988).

The regional north-south folding observed in western Norway, if accurately placed as latest Devonian–earliest Carboniferous in age, conforms very well with inversion, igneous activity, extensional basin formation, and unconformities documented around the North Atlantic margin. In the United Kingdom, folds in the Devonian Old Red

Sandstone of the Orcadian and East Shetland basins have been presumed to be of latest Devonian ages. This activity was followed by block faulting in central England and Scotland and thick Lower Carboniferous sedimentary basin fill, as well as initiation of alkaline and tholeiitic volcanism of Visean-Tournaisian age (Midland Valley region) (Francis 1983; Cameron and Stephenson 1985; Gatliff et al. 1994). Plutonic activity on Shetland of Early Carboniferous age (Torsvik et al. 1989) appears to have followed closely on folding of Devonian strata in the ORS. Similarly, in Svalbard, Early Carboniferous faulting and basin formation succeeded Late Devonian folding of ORS sediments (Harland et al. 1984; Bergh et al. 1997). On East Greenland, a recently identified major Early Carboniferous unconformity (pre–336 Ma) in a formerly "Devonian" basin (Hartz et al. 1997) attests to a tectonically induced erosional (or nondepositional) episode in the area, possibly associated with local magmatic activity. A major sedimentary hiatus of latest Devonian–Early Carboniferous age has also been described for the northern Siberian platform (Nishikin et al. 1996). Events of similar age in western Norway should not be unexpected, but were not recognized previously simply because of the lack of rocks younger than Middle Devonian in the area. The application of alkali feldspar $^{40}Ar/^{39}Ar$ thermochronology and MDD analysis to understand late Paleozoic tectonics in Baltica has recently been demonstrated in a regional transect in southern Norway (south of the present study) and has identified a Late Carboniferous (270–330 Ma) cooling event attributed to regional lowering of base level because of onset of rifting in the Oslo Graben (Dunlap and Fossen 1998).

Various postulates for the broader "tectonic regime" responsible for the Late Devonian–Early Carboniferous folding, faulting, magmatism, and/or unroofing and erosion have been proposed. Several groups have suggested direct relation to continuation/enhancement of the transcurrent motion along the Laurentia-Baltica suture, with a locus perhaps along the Møre-Trøndelag Fault Complex, following on oblique Caledonian collision (Harland et al. 1984; Torsvik et al. 1996; Krabbendam and Dewey 1998; Osmundsen et al. 1998). Others have invoked or included more long-wavelength, external factors like back-arc extension related to subduction of the Rheic Ocean as the European Massifs and Gondwana advanced north toward Euramerica or as a response from the docking of Kazakhstan from the east (e.g., Torsvik et al. 1990). At this time, we lack strong evidence to support a single external tectonic event and, indeed, they may be interrelated. Regardless, the driving mechanism for western Norway rapid cooling must incorporate latest Devonian–Early Carboniferous folding and increased topography.

## Conclusion

The consistency in modeling results from feldspars representing different tectonostratigraphic levels and rock types supports the thermal histories calculated with the MDD approach. The results are further supported by independently determined geologic evidence: the onset of rapid cooling in the Early Carboniferous in western Norway, determined by the feldspar modeling, is contemporaneous with other, similar faulting episodes, unconformities, and magmatic production around the North Atlantic margin. The cause for rapid cooling in western Norway is attributed to topographic/erosive response to a thermal pulse/underplating beneath Baltica in latest Devonian time, accompanied by folding along east-west axes. The latter folding postdates Early-Middle Devonian basin formation in western Norway and may be linked to sinistral shearing along the More-Trondelag Fault Zone.

Despite the apparent success of the MDD approach in describing feldspar thermal histories in some geologic settings, research heretofore has not yet generated a thorough understanding of diffusion through complex feldspar microtextures and the microtextures' bearing on the physical manifestations of feldspar "domains." Combined field and experimental studies focusing on microtextures and their behavior during laboratory heating will be critical to address these fundamental aspects of the modeling technique.

### ACKNOWLEDGMENTS

The research in this study was largely possible through the Geological Survey of Norway project "Onshore-Offshore Tectonic Links in Western Norway: An Integrated Approach," supported financially by Mobil Exploration Norway, Phillips Petroleum, and Statoil. Additional funding to T. B. Andersen was provided by Norsk Agip. The article benefited greatly from contrasting and constructive reviews from two anonymous referees.

## REFERENCES CITED


Andersen, T. B. 1998. Extensional tectonics in the Caledonides of southern Norway, an overview. Tectonophysics 285:333–351.

Andersen, T. B.; Berry, H. N., IV; Lux, D. R.; and Andresen, A. 1998. The tectonic significance of pre-Scandian $^{40}Ar/^{39}Ar$ phengite cooling ages in the Caledonides of Western Norway. J. Geol. Soc. Lond. 155:297–310.

Andersen, T. B., and Jamtveit, B. 1990. Uplift of deep crust during orogenic extensional collapse: a model based on field studies in the Sogn-Sunnfjord region of western Norway. Tectonics 9:1097–1111.

Andersen, T. B.; Jamtveit, B.; Dewey, J. F.; and Swensson, E. 1991. Subduction and eduction of continental crust: major mechanisms during continent-continent collision and orogenic extensional collapse. Terra Nova 3: 303–310.

Andersen, T. B.; Osmundsen, P.-T.; and Jolivet, L. 1994. Deep crustal fabrics and a model for the extensional collapse of the southwest Norwegian Caledonides. J. Struct. Geol. 16:1191–1203.

Arnaud, N. O.; Brunel, M.; Cantagrel, J. M.; and Tapponier, P. 1993. High cooling and denudation rates at Kongur Shan, eastern Pamir (Xinjiang, China) revealed by $^{40}Ar/^{39}Ar$ alkali feldspar thermochronology. Tectonics 12:1335–1346.

Arnaud, N. O., and Eide, E. A. 1998. Brecciation-related argon redistribution in K-feldspars: an in naturo crushing study. Mineral. Mag. 62A:67–68 (abstract).

Arnaud, N. O., and Kelley, S. P. 1997. Argon behaviour in gem-quality orthoclase from Madagascar: experiments and some consequences for $^{40}Ar/^{39}Ar$ geochronology. Geochim. Cosmochim. Acta 61:3227–3255.

Bergh, S. G.; Braathen, A.; and Andresen, A. 1997. Interaction of basement-involved and thin-skinned tectonism in the Teritary fold-thrust belt of central Spitsbergen, Svalbard. Am. Assoc. Petrol. Geol. Bull. 81: 637–661.

Berry, H. N., IV; Lux, D. R.; Andresen, A.; and Andersen, T. B. 1995. Progressive exhumation during orogenic collapse as indicated by $^{40}Ar/^{39}Ar$ cooling ages from different structural levels, southwest Norway. Geonytt 22:20–21 (abstract).

Bøe, R., and Bjerkli, K. 1989. Mesozoic sedimentary rocks in Edøyfjorden and Beitstadfjorden, central Norway: implications for the structural history of the Møre Trøndelag fault zone. Mar. Geol. 87:287–299.

Boundy, T. M.; Essene, E. J.; Hall, C. M.; Austrheim, H.; and Halliday, A. N. 1996. Rapid exhumation of lower crust during continent-continent collision and late extension: evidence from $^{40}Ar/^{39}Ar$ incremental heating of hornblendes and muscovites, Caledonian orogen, western Norway. Geol. Soc. Am. Bull. 108:1425–1437.

Brekke, H., and Solberg, P. O. 1987. The geology of Atløy, Sunnfjord, western Norway. Nor. Geol. Unders. Bull. 410:73–94.

Burgess, R.; Kelley, S. P.; Parsons, I.; Walker, F. D. L.; and Worden, R. H. 1992. $^{40}Ar$-$^{39}Ar$ analysis of perthite microtextures and fluid inclusions in alkali feldspars from the Klokken syenite, South Greenland. Earth Planet. Sci. Lett. 109:147–167.

Cameron, I. B., and Stephenson, D. 1985. The Midland Valley of Scotland (3d ed.). London, Her Majesty's Stationery Office, Brit. Geol. Surv./Natural Environ. Res. Council, 172 p.

Cebula, G. T.; Kunk, M. J.; Mehnert, H. H.; Naeser, C. W.; Obradovich, J. D.; and Sutter, J. F. 1986. The Fish Canyon Tuff, a potential standard for the $^{40}Ar$-$^{39}Ar$ and fission-track dating methods. Terra Cognita Proc. Intl. Conf. Geochron. IV 6:139–140 (abstract).

Chauvet, A., and Séranne, M. 1994. Extension-parallel folding in the Scandinavian Caledonides: implications for late-orogenic processes. Tectonophysics 238: 31–54.

Copeland, P.; Harrison, T. M.; Hodges, K. V.; Maruéjol, P.; LeFort, P.; and Pecher, A. 1991. An Early Pliocene thermal disturbance of the Main Central Thrust, Central Nepal: implications for Himalayan tectonics. J. Geophys. Res. 96:8475–8500.

Coward, M. P. 1993. The effect of Late Caledonian and Variscan continental escape tectonics on basement structure, Paleozoic basin kinematics and subsequent Mesozoic basin development in NW Europe. *In* Parker, J. R., ed. Petroleum geology of northwest Europe: proceedings of the fourth conference. Geological Society, London, p. 1095–1108.

Cuthbert, S. J. 1991. Evolution of the Devonian Hornelen Basin, western Norway: new constraints from petrological styudies of metamorphic clasts. *In* Morton, A. C.; Todd, S. P.; and Haughton, P. D. W., eds. Developments in sedimentary provenance studies. Geol. Soc. London Spec. Publ. 57:343–360.

Cuthbert, S. J., and Carswell, D. A. 1990. Formation and exhumation of medium-temperature eclogites in the Scandinavian Caledonides. *In* Carswell, D. A., ed. Eclogite facies rocks. Glasgow, Blackie & Son, p. 180–203.

Dewey, J. F.; Ryan, P. D.; and Andersen, T. B. 1993. Orogenic uplift and collapse, crustal thickness, fabrics and metamorphic phase changes: the role of eclogites. *In* Alabaster, H. M.; Harris, N. B. W.; and Neary, C. R., eds. Magmatic processes and plate tectonics. Geol. Soc. London Spec. Publ. 76:325–343.

Dobrzhinetskaya, L. F.; Eide, E. A.; Larsen, R. B.; Sturt, B. A.; Trønnes, R. G.; Smith, D. C.; Taylor, W. R.; and Posukhova, T. V. 1995. Microdiamond in high-grade metamorphic rocks of the Western Gneiss Region, Norway. Geology 23:597–600.

Dodson, M. H. 1973. Closure temperature in cooling geochronological and petrological systems. Contrib. Mineral. Petrol. 40:259–274.

Dunlap, W. J., and Fossen, H. 1998. Early Paleozoic orogenic collapse, tectonic stability, and late Paleozoic

continental rifting revealed through thermochronology of K-feldspars, southern Norway. Tectonics 17: 604–620.

Eide, E. A.; Torsvik T. H.; and Andersen, T. B. 1997. Absolute dating of brittle fault movements: Late Permian and late Jurassic extensional fault breccias in western Norway. Terra Nova 9:135–139.

Færseth, R. B. 1996. Interaction of Permo-Triassic and Jurassic extensional fault-blocks during the development of the northern North Sea. J. Geol. Soc. Lond. 153:931–944.

Færseth, R. B.; Macintyre, R. M.; and Naterstad, J. 1976. Mesozoic alkaline dykes in the Sunnhordaland region, western Norway: ages, geochemistry and regional significance. Lithos 9:331–345.

Foland, K. A. 1974. $^{40}$Ar diffusion in homogeneous orthoclase and an interpretation of Ar diffusion in K-feldspar. Geochim. Cosmochim. Acta 38:151–166.

Foland, K. A., and Xu, Y. 1990. Diffusion of $^{40}$Ar and $^{39}$Ar in irradiated orthoclase. Geochim. Cosmochim. Acta 54:3147–3158.

Fossen, H. 1992. The role of extensional tectonics in the Caledonides of South Norway. J. Struct. Geol. 14: 1033–1046.

Fossen, H., and Dunlap, W. J. 1998. Timing and kinematics of Caledonian thrusting and extensional collapse, southern Norway: evidence from $^{40}$Ar/$^{39}$Ar thermochronology. J. Struct. Geol. 20:765–781.

Fossen, H.; Mangerud, G.; Hesthammer, J.; Bugge, T.; and Gabrielsen, R. H. 1997. The Bjorøy Formation: a newly discovered occurrence of Jurassic sediments in the Bergen Arc System. Norsk Geol. Tidsskr. 4:269–287.

Francis, E. H. 1983. Carboniferous. *In* Craig, G. Y., ed. Geology of Scotland. Edinburgh, Scottish Academic, p. 297–320.

Gaber, L. J.; Foland, K. A.; and Corbato, C. 1988. On the significance of argon release from biotite and amphibole during $^{40}$Ar/$^{39}$Ar vacuum heating. Geochim. Cosmochim. Acta 52:2457–2465.

Gatliff, R. W.; Richards, P. C.; Smith, K.; Graham, C. C.; McCormac, M.; Smith, N. J. P.; Long, D.; et al. 1994. The geology of the central North Sea. Brit. Geol. Surv. U.K. Offshore Reg. Rep. London, Her Majesty's Stationery Office, 118 p.

Gradstein, F. M., and Ogg, J. G. 1996. A Phanerozoic time scale. Episodes 19:3–5.

Gromet, L. P., and Andersen, T. B. 1994. Eclogite inclusions in granite gneisses: preservation of Precambrian intrusive relations in the eclogitized crust of Sunnfjord, SW Norway. Geol. Soc. Am. Abstr. Program 26: 198 (abstract).

Hames, W. E., and Bowring, S. A. 1994. An empirical evaluation of the argon diffusion geometry in muscovite. Earth Planet. Sci. Lett. 124:161–167.

Harland, W. B.; Gaskell, B. A.; Heafford, A. P.; Lind, E. K.; and Perkins, P. J. 1984. Outline of Arctic post-Silurian continental displacements. *In* Spencer, A. M.; Holter E.; Johnsen, S. O.; Mørk, A.; Nysaether, E.; Songstad, P.; and Spinnangr, Å, eds. Petroleum geology of the north European margin. London, Graham & Trotman, p. 137–148.

Harrison, T. M.; Lovera, O. M.; and Heizler, M. T. 1991. $^{40}$Ar/$^{39}$Ar results for alkali feldspars containing diffusion domains with differing activation energy. Geochim. Cosmochim. Acta 55:1435–1448.

Hartz, E. H., and Andresen, A. 1997. From collision to collapse: complex strain permutations in the hinterland of the Scandinavian Caledonides. J. Geophys. Res. 102:24,697–24,711.

Hartz, E. H.; Torsvik, T. H.; and Andresen, A. 1997. Carboniferous age for the East Greenland "Devonian" basin: paleomagnetic and isotopic constraints on age, stratigraphy, and plate reconstructions. Geology 25: 675–678.

Haszeldine, R. S. 1984. Carboniferous North Atlantic palaeogeography: stratigraphic evidence for rifting, not megashear or subduction. Geol. Mag. 121:443–463.

Hossack, J. R. 1984. The geometry of listric growth faults in the Devonian basins of Sunnfjord, W. Norway. J. Geol. Soc. Lond. 141:629–637.

Hurich, C., and Kristoffersen, Y. 1988. Deep structure of the Caledonide Orogen in southern Norway: new evidence from marine seismic reflection profiling. *In* Kristofferson, Y., ed. Progress in studies of the lithosphere in Norway. Nor. Geol. Unders. Spec. Publ. No. 3, p. 96–101.

Kolderup, C. F. 1921. Kvamshestens devonfelt. Bergens Mus. Aarb. 1920–1921, Naturvid. Rk. 4, 96 pp.

Krabbendam, M., and Dewey, J. 1998. Exhumation of UHP rocks by transtension in the Western Gneiss Region, Scandinavian Caledonides. *In* Holdsworth, R. E., Strachan, R. A.; and Dewey, J. F., eds. Continental transpressional and transtensional tectonics. Geol. Soc. London Spec. Publ. 135, p. 159–181.

Lovera, O. M. 1990. Computer programs to model $^{40}$Ar/$^{39}$Ar diffusion data from multidomain samples. Comp. Geosci. 18:789–813.

Lovera, O. M.; Grove, M.; Harrison, T. M.; and Mahon, K. I. 1997. Systematic analysis of K-feldspar $^{40}$Ar/$^{39}$Ar heating results. I. Significance of activation energy determinations. Geochim. Cosmochim. Acta 61: 3171–3192.

Lovera, O. M.; Richter, F. M.; and Harrison, T. M. 1989. The $^{40}$Ar/$^{39}$Ar thermochronometry for slowly cooled samples having a distribution of diffusion domain sizes. J. Geophys. Res. 94:17,917–17,935.

———. 1991. Diffusion domains determined by $^{39}$Ar released during step heating. J. Geophys. Res. 96: 2057–2069.

Løvlie, R., and Mitchell, J. G. 1982. Complete remagnetization of some Permian dykes from western Norway induced during burial/uplift. Phys. Earth Plan. Int. 30:415–421.

Maluski, H. 1996. Argon 40–argon 39 dating: principles and applications to minerals from terrestrial rocks. *In* Roth, E., and Poty, B., eds. Nuclear methods of dating. Dordrecht, Kluwer Academic, p. 325–351.

Manckelow, N. S., and Grasemann, B. 1997. Time-dependent effects of heat advection and topography

on cooling histories during erosion. Tectonophysics 270:167–195.

McDougall, I., and Harrison, T. M. 1988. Geochronology and thermochronology by the $^{40}Ar/^{39}Ar$ method. New York, Oxford University Press, 215 p.

Nikishin, A. M.; Ziegler, P. A.; Stephenson, R. A.; Cloetingh, S. A. P. L.; Furne, A. V.; Fokin, P. A.; Ershov, A. V.; et al. 1996. Late Precambrian to Triassic history of the East European Craton: dynamics of sedimentary basin evolution. Tectonophysics 268:23–63.

Osmundsen, P.-T., and Andersen, T. B. 1994. Caledonian compressional and late-orogenic extensional deformation in the Staveneset area, Sunnfjord, western Norway. J. Struct. Geol. 10:1385–1401.

Osmundsen, P.-T.; Andersen, T. B.; Markussen, S.; and Svendby, A. K. 1998. Tectonics and sedimentation in the hanging wall of a major extensional detachment: the Devonian Kvamshesten Basin, western Norway. Basin Res. 10:213–234.

Richter, F. M.; Lovera, O. M.; Harrison, T. M.; and Copeland, P. 1991. Tibetan tectonics from $^{40}Ar/^{39}Ar$ analysis of a single K-feldspar sample. Earth Planet. Sci. Lett. 105:266–278.

Roberts, D. 1983. Devonian tectonic deformation in the Norwegian Caledonides and its regional perspectives. Nor. Geol. Unders. Bull. 380:85–96.

Rohrman, M.; van der Beek, P.; and Andriessen, P. 1994. Syn-rift thermal structure and post-rift evolution of the Oslo Rift (southeast Norway): new constraints from fission track thermochronology. Earth Planet. Sci. Lett. 127:39–54.

Rohrman, M.; van der Beek, P.; Andriessen, P.; and Cloetingh, S. 1995. Meso-Cenozoic morphotectonic evolution of southern Norway: Neogene domal uplift inferred from apatite fission track thermochronology. Tectonics 14:704–718.

Smith, D. C. 1984. Coesite in clinopyroxene in the Caledonides and its implications for geodynamics. Nature 310:641–644.

Steel, R. J., and Worsley, D. 1984. Svalbard's post-Caledonian strata—an atlas of sedimentational patterns and paleogeographic evolution. *In* Spencer, A. M.; Holter E.; Johnsen, S. O.; Mørk, A.; Nysaether, E.; Songstad, P.; and Spinnangr, Å., eds. Petroleum geology of the north European margin. London, Graham & Trotman, p. 109–135.

Sundvoll, B., and Larsen, B. T. 1994. Architecture and early evolution of the Oslo Rift. Tectonophysics 240: 173–189.

Torsvik, T. H.; Andersen, T. B.; Eide, E. A.; and Walderhaug, H. 1997. The age and tectonic significance of dolerite dykes in western Norway. J. Geol. Soc. Lond. 154:961–973.

Torsvik, T. H.; Smethurst, M. A.; Briden, J. C.; and Sturt, B. A. 1990. A review of Palaeozoic palaeomagnetic data from Europe and their palaeogeographical implications. *In* McKerrow, W. S., and Scotese, C. R., eds. Palaeozoic palaeogeography and biogeography. Geol. Soc. Lond. 12:25–41.

Torsvik, T. H.; Smethurst, M. A.; Meert, J. G.; Van der Voo, R.; McKerrow, W. S.; Brasier, M. D.; Sturt, B. A.; and Walderhaug, H. J. 1996. Continental break-up and collision in the Neoproterozoic and Palaeozoic—a tale of Baltica and Laurentia. Earth-Sci. Rev. 40:229–258.

Torsvik, T. H.; Sturt, B. A.; and Ramsay, D. M. 1989. On the origin and the tectonic implications of magnetic overprinting of the Old Red Sandstone, Shetland. Geophys. J. Int. 99:749–759.

Torsvik, T. H.; Sturt, B. A.; Ramsay, D. M.; Kisch, H. J.; and Bering, D. 1986. The tectonic implications of Solundian (Upper Devonian) magnetization of the Devonian rocks of Kvamshesten, western Norway. Earth Plan. Sci. Lett. 80:337–347.

Torsvik, T. H.; Sturt, B. A.; Swensson, E.; Andersen, T. B.; and Dewey, J. F. 1992. Palaeomagnetic dating of fault rocks: evidence for Permian and Mesozoic movements and brittle deformation along the extensional Dalsfjord Fault, western Norway. Geophys. J. Int. 109: 565–580.

Tucker, R. D.; Bradley, D. C.; Ver Straeten, C. A.; Harris, A. G.; Ebert, J. R.; and McCutcheon, S. R. 1998. New U-Pb zircon ages and the duration and division of Devonian time. Earth Planet. Sci. Lett. 158:175–186.

Villa, I. 1994. Multipath Ar transport in K-feldspar deduced from isothermal heating experiments. Earth Planet. Sci. Lett. 122:393–401.

Wain, A. 1997. New evidence for coesite in eclogite and gneisses: defining an ultrahigh-pressure province in the Western Gneiss region of Norway. Geology 25: 927–930.

Ziegler, P. A. 1990. Geological atlas of western and central Europe. Mijdrecht, Shell Internationale Petroleum Maatschappij B.V., 239 p.